Acta Materialia xxx (2017) xxx-xxx

Contents lists available at ScienceDirect

Acta Materialia

journal homepage: www.elsevier.com

Full length article

Elastocaloric cooling capacity of shape memory alloys – Role of deformation temperatures, mechanical cycling, stress hysteresis and inhomogeneity of transformation

Y. Wu, E. Ertekin, H. Sehitoglu

Department of Mechanical Science and Engineering, University of Illinois at Urbana-Champaign, 1206 W. Green St., Urbana, IL 61801, USA

ARTICLE INFO

Article history:
Received 14 February 2017
Received in revised form 1 June 2017
Accepted 3 June 2017
Available online xxx

Keywords:
Elastocaloric (EC) effect
Superelasticity (SE)
Entropy change
Temperature span
Functional fatigue resistance
Hysteresis

ABSTRACT

Elastocaloric (EC) effect refers to the rapid cooling in shape memory alloys (SMAs) during reverse transformation from martensite to austenite under adiabatic conditions. We present a very comprehensive study of the EC response far extending the existing literature by studying the effect of loading states (tension and compression), long-term cycling, strain localization, and deformation temperatures in several SMAs including CuZnAl, NiTi, NiTiCu, Ni_2FeGa and $NiTiHf_{13.3}$. We found a temperature change of 14.2 °C in CuZnAl, 18.2 °C in NiTi, 15.2 °C in NiTiCu, 13.5 °C in Ni_2FeGa, and 6.95 °C in $NiTiHf_{13.3}$ upon reverse transformation depending on the entropy change (as high as 60 J/kg K), the stress hysteresis, the inhomogeneity of the transformation and the number of superelastic cycles. A gradual deterioration of the EC effect in tension develops, while in compression the EC effect can be sustained much longer (in excess of 10^4 cycles). The Ni_2FeGa SMAs possess an operational EC temperature window of nearly 200 °C, which is the widest among the chosen SMAs. With over one hundred experiments reported in one study, this paper represents an authoritative summary of the EC capabilities of a wide range of SMAs.

1. Introduction

1.1. Background and motivation

Shape memory alloys (SMAs) are an intriguing class of metallic materials owing to their unique functional responses (superelasticity (SE) and shape memory effect (SME)) and have been studied in depth over the last three decades. Recently, the 'elastocaloric (EC)' properties of SMAs has opened potentially new applications and some preliminary EC cooling prototypes have been designed and tested as well [1–3]. The EC effect originates from the entropy change associated with the reverse (endothermic) martensitic phase transformation upon the removal of an external stress field. Under adiabatic conditions, the material cools down considerably and, afterwards, it absorbs heat from the surrounding. During this process, the temperature changes can be profound (25 °C in NiTi [3–5]) far exceeding those achieved with magnetocaloric rare earth materials. However, the effects of long-term cycling, the role of deformation temperatures, and the adverse effects of strain localization on the EC properties are still not well understood. The current paper represents an extensive treatise on the EC response for multiple SMAs, including NiTi, NiTiCu, Ni_2FeGa, CuZnAl, and NiTiHf single crystals. The EC studies so far have been undertaken on CuZnAl [6], NiTi [4,7], and NiTi-based SMAs [3,7,8]. We extend the understanding on other SMAs and explore potential operation capabilities at multiple temperatures. Most studies [9] have explored the topic mainly at room temperature and over finite number (i.e. < 100 cycles) of load-unload cycles under tension. Comprehensive experimental efforts encompassing multiples cycles (exceeding 10^4 cycles), different temperature levels, and load states (tension and compression) for multiple SMAs have not been undertaken in a single study. This paper aims to fulfill this need.

Although it has been well established that the EC effect is manifested through the entropy change under adiabatic conditions [10], two other considerations are equally noteworthy. These are whether the SE response and EC effect, which are intrinsically linked, are stable under multi-cycles [6] and whether such an effect can be realized over a range of deformation temperatures (the span of EC window). To exemplify, let us consider the NiTi binary alloy that is regarded as one of the most promising materials for EC application. It has been found that the giant caloric effect of NiTi can elicit a temperature change near 25 °C due to very large entropy change of 50 J/kg K [11]. However, the functional degradation of SE, hence EC effect, over multi-cycles can be substantial in this class of material [7,8,12]. To be more specific, the temperature change decreases by approximately 40% after the first 100 cycles [8]. Another concern with NiTi is that the SE temperature window is less than 50 °C [13], which corresponds to a narrow EC span. Understanding the effect of deformation temperature on EC response is imperative for applications where

Corresponding author.
Email address: huseyin@illinois.edu (H. Sehitoglu)

http://dx.doi.org/10.1016/j.actamat.2017.06.012
1359-6454/

giant cooling capabilities at elevated temperatures are desired. Therefore, the SMAs that exhibit high entropy changes, good functionality under multi-cycles (i.e. small dissipation and repeatability of transformation response), and a wide deformation temperature window for SE constitute superior potential for the EC performance. We will elaborate on the specific issues in the following section.

The existence of hysteresis is intrinsic to first-order phase transformation, and is also unavoidable and detrimental to the EC performance of SMAs. The hysteresis originates from the energy dissipation in the form of frictional work and plastic accommodation [14]. The former is spent overcoming the resistance to interfacial motion between parent and product phase and the latter occurs when the coherency strains of martensite-austenite interface relax. It is evident that smaller hysteresis corresponds to less energy dissipation, which is also undoubtedly beneficial for optimizing EC properties of SMAs. In the case of NiTi, the hysteresis can either expand or shrink when the sample is deformed at elevated temperatures depending on Ni content [14,15]. Therefore, it is anticipated that such hysteresis change may affect its cooling capacity. However, the experimental evidence regarding the connection between hysteresis and EC properties is still lacking. At present, a recent study [16] on NiTi wire associated with the B2↔R and B2↔B19′ transitions has pointed out that the reduced hysteresis is expected to optimize the EC response. Nonetheless, a systematic study on the correlation between the stress hysteresis variation with the deformation temperature and the corresponding EC effect is not sufficiently available in the literature. In this work, we will provide elucidation on this issue.

Another consideration in the EC properties of SMAs is the role of strain localization. Its adverse effect in fatigue and fracture has been well known [17]. In SMAs, the strain localization can be an outcome of the inhomogeneous phase transformation [18–21]. The large strain accumulated at local regions where the transformation zone is confined may induce slip-mediated plastic deformation [21]. This can impose serious limitations to the recoverability of SMAs and therefore diminishing the efficacy of their EC performance. The origin of such strain heterogeneity is partly attributed to the difficulty of the migration of interfaces where the energy barriers governing migration can differ from nucleation [22,23]. The heterogeneous nature of the phase transformation in SMAs can produce a non-uniform temperature distribution across the material, which may compromise their cooling efficiency. The characterization of the EC effect with respect to the strain distribution is still an ongoing research effort. The non-uniform temperature profiles were first reported in the CuZnAl single crystallines [24] and the NiTi wires [5] using thermography. Both of these works pinpointed the role of localized nature of phase transformation. Recent works on NiTi [25] and NiTiCuCo [7] thin films have utilized the in-situ digital image correlation (DIC) in conjunction with infrared (IR) thermography to unveil the relationship between the spatial distributions of strain and temperature contours during deformation. They confirmed the inhomogeneous temperature field in correspondence to the heterogeneous strain distribution across the sample. In this paper, we reveal the correlation between the strain heterogeneity and the EC effect for five important SMAs using DIC and IR thermography. The former was also quantified via strain histograms based on the DIC strain measurement. Particularly in the case of $NiTiHf_{13.3}$, we found that the effect of strain inhomogeneity on its EC performance is rather severe. We will elaborate on this later.

Unlike most previous works, the present study utilizes single crystals to obtain results without the role of grain boundaries and for which transformation fronts are well defined to measure temperature and strain variations. We consider the EC effects in five contemporary SMAs at numerous temperatures and long-term load cycles under both tensile and compressive loading states. By studying compression in addition to tension, we uncover the modified EC responses corresponding to different stress/strain levels, temperature regimes, and hysteresis.

1.2. Achieving superior EC response in SMAs

As aforementioned, the desired properties of materials utilized for EC are threefold: (a) a large entropy change during the stress-induced phase transformation, (b) a good functional fatigue response, and (c) a wide SE temperature span. The temperature change, ΔT, arising from the reversible transformation between crystal phases has a direct correlation to the entropy change, ΔS, as $\Delta T = -\frac{T}{C_p}\Delta S(T)$ [6], where C_p is the specific heat capacity and T is the test temperature. Thereby, the ΔS is a vital parameter, which governs the maximum potential ΔT achievable. From this perspective, NiTi-based SMAs are the most favorable due to their high ΔS [11]. The corresponding adiabatic ΔT is also substantial – 14 °C for bulk material [11] and 17 °C for thin film [3]. In addition to NiTi-based alloys, a summary of ΔS was established for a broad range of SMAs in this work to gain an insight into their maximum cooling capabilities.

Secondly, characterizing functional fatigue resistance is another important factor that can shed light into the EC performance of SMAs. Materials with better functional fatigue impedance are believed to demonstrate stable EC performance [10]. Thus, it is imperative to investigate the former first and attempt to establish such a correlation experimentally for a wide range of materials. Previously, such correlation has been constructed for NiTi over hundreds of cycles in tension [5,7,8]. However, NiTi alloys can suffer from short fatigue lives at 4% of strain [12,26] and their EC cooling capacity was found to degrade rapidly over successive cycles due to excessive plasticity [7]. Compared to NiTi, CuZnAl and Ni_2FeGa alloys have demonstrated longer fatigue lives exceeding 10^4 cycles at a 10% strain and better functional stability [27,28]. Thereby, it is expected that the EC performance of CuZnAl and Ni_2FeGa would be better. A preliminary study on polycrystalline CuZnAl has demonstrated promising reproducibility of temperature change over 16 cycles [6]. However, the variation of the cooling capability with successive loading cycles is still needed. Hence, a detailed study of their EC responses in excess of 10^4 cycles would provide further evidence regarding the effect of load cycles on EC performance.

Thirdly, a large EC temperature window is another desired feature, as the solid refrigerant needs to accommodate different temperature conditions in practice. In the foregoing studies, the temperature spans associated with the EC effect of FeRh [29], CuZnAl [6], FePb [30], NiFeGaCo [31], and NiMnInCo [32] have been established. Among all, the polycrystalline CuZnAl showed the broadest temperature span of the order of 130 °C. In this study, we constructed the EC windows for five important SMAs with particular emphasis on Ni_2FeGa alloys that have high temperature capabilities.

Furthermore, the study of EC performance under compressive stress can open up new possibilities. It is known that the mechanical fatigue under compression is superior since the propagation of a crack can be retarded and therefore a prolonged life span is likely to occur [4]. Hence, studying EC effects under compression has conspicuous merits and high potentials. However, the majority of the available experimental undertakings has focused on the EC effects under tensile loading only [6,7,11,25]. In this work, we invest considerable endeavors on the efficacy of the chosen SMAs under compression, because SE, hence EC behavior, is expected to be different compared to those in tension.

1.3. Overview of previous work and background on the SMAs

In our previous work [11], we showed the efficacy of NiTi, Ni_2FeGa and CoNiAl for two repeated cycles, with CoNiAl operating at 100 °C but with small temperature change. In this study, we expanded our focus on five different SMA single crystals, namely CuZnAl, Ni_2FeGa, NiTi, NiTiCu, and $NiTiHf_{13.3}$. To be more specific, we selected single crystal orientations that correspond to superior shape memory strains - [001] CuZnAl, [001] Ni_2FeGa, [111] $NiTiHf_{13.3}$, and [148] NiTi in tension, and [001] NiTiCu, [148] NiTi, [001] CuZnAl, and [001] Ni_2FeGa in compression. For NiTi, the choice of [148] was to optimize the compressive response because the transformation strain is the highest near [148] pole in compression [33]. This orientation does not produce the most favorable response in tension. Since our aim was to utilize the same orientation in both tension and compression. The choice of [148] achieved our goal in this sense.

Among all, NiTi, NiTiCu, and $NiTiHf_{13.3}$ SMAs have substantial entropy changes during the reversible phase transformation with $NiTiHf_{13.3}$ exceeding 50 J/kg K [20]. In addition, we chose NiTi with higher Ni concentration (50.8 at.%) as opposed to earlier literature [4,7,8], because the Ni-rich material shows smaller changes in superelasticity upon cyclic deformation [12]. Compared to the NiTi-based SMAs, CuZnAl and Ni_2FeGa have lower entropy changes [11]. However, they exhibit much lower hysteresis and good functional stability of SE under multi-cycles at a strain range of 10% [27,28] so are expected to possess good EC properties. In addition, Ni_2FeGa SMAs exhibit SE over a wide temperature window- from 10 °C to 340 °C [34]. Therefore, the Ni_2FeGa alloys could be favored for EC cooling applications, especially at high temperatures, compared to other SMAs.

1.4. Basic outline of the current research

The basic outline of the current research is demonstrated in Fig. 1. Experimentally, the temperature profiles were measured over multi-cycles (>10^4 cycles) as shown in Fig. 1a and b. The stress hysteresis, $\Delta\sigma$, is defined as the difference between the upper and lower stress plateau at the middle of a hysteresis loop [14] (see arrows in Fig. 1a). The spatial temperature and strain levels were determined by the thermography and digital image correlation respectively. Such spatial temperature measurements (including the specimen gage section and surrounding grip sections) are important to ensure that adiabatic conditions are indeed present for the high unloading rates. These experimentally measured temperature changes (ΔT) were then compared to the predicted values (ΔT_{th}) computed from the entropy changes in order to gain an insight into the differences. Both the experimentally measured Clausius-Clapeyron slopes and the latent heat determined from differential scanning calorimetry (DSC) [35] were used to calculate the entropy change of each material as shown in Fig. 1c and d. The calculation process of the temperature change prediction will be elaborated in the result section. During the uniaxial tensile experiment, a dual camera system was set up to capture images for strain [36] and temperature measurement simultaneously. A comparison was made between the strain field measured from DIC and thermography in order to seek a correlation between transformation domains and temperature gradients. The temperature dependence of the EC effect was also investigated and the results are presented for the five materials. The stability of ΔT over consecutive cycles is also discussed in this paper. In summary, the current investigation provides a timely contribution to the EC response of SMAs fulfilling requisite knowledge on the effect of cyclic loading, hysteresis, strain localization, and deformation temperatures.

2. Methodology

2.1. Materials

The nominal composition, heat treatment, specific heat capacity (C_p), and phase transformation for each of the five materials are included in Table 1. The single crystals were grown using Bridgeman technique in an inert environment. The ingots of each material were then sectioned into multiple dog-bone tensile specimen with a dimension of 1.5 mm × 3 mm x 10mm in the gauge section using electrical discharge machine (EDM). The compression samples were sectioned with a dimension of 4 mm × 4 mm x 8mm. The transformation temperatures were measured via a Perkin Elmer Pyris 1 DSC machine with a scan rate of 40 °C/min. The specific heat capacities were determined using ASTM standard E1269 for each material.

2.2. Experiments

Prior to any experiments, the oxidation and damage from EDM cutting on the surface were mechanical polished to a mirror finishing with abrasive papers up to P1800 grit. Thin foils, 30 mg–40 mg, were cut using a low speed diamond saw for transformation temperature characterization using DSC. On the surfaces of the small-scale tensile specimens, a fine speckle pattern was airbrushed on one side of the specimen for DIC and a black paint was applied on the other side for IR imaging.

The uniaxial tensile experiments were performed on an Instron servo hydraulic load frame at different temperatures. The temperatures of the samples were adjusted by heating the grips with variable heating tapes. The load frame was controlled by a customized LabView program with the ability to take images automatically. The images for DIC were taken by an IMI-202FT digital camera with a maximum frame rate of 15 fps and have uniform dimensions of 1600 pixels × 1200 pixels. An area of 3 mm × 6 mm was captured by the DIC camera with a resolution of 4.25μm/pix. The DIC strain field within this area of interest was determined using a commercial software VIC-2D by correlating the deformed images with the reference image. On the other side of the sample where black paint was applied, a DeltaTherm 1550 infrared camera was setup for IR imaging. The maximum frame rate of this IR system is up to 1000 fps and the image captured has a dimension of 320 pixels × 256 pixels. The IR system was calibrated in a temperature range of 15 °C to 200 °C.

Specimens underwent double-damp loading. They were loaded at very a low strain rate of 2×10^{-3} s^{-1} for CuZnAl and Ni_2FeGa and 2×10^{-4} s^{-1} for NiTi, $NiTiHf_{13.3}$, and NiTiCu to prevent excessive self-heating due to the exothermic forward phase transformation. The unloading process was performed at a faster strain rate of 0.2 s^{-1} in order to approach adiabatic condition. With the dual camera system being set up, the entire loading and unloading process was recorded by both cameras. Therefore, the strain and temperature values at different load levels were obtained. Subsequently, the DIC strain contours were compared with the temperature gradient to gain an insight into the correlation between transformation and temperature changes.

3. Results

We first introduce the results of CuZnAl, Ni_2FeGa, and NiTi from Sections 3.1–3.3 followed by those of NiTiCu and NiTiHf in Section 3.4. The effect of the deformation temperature on their EC properties

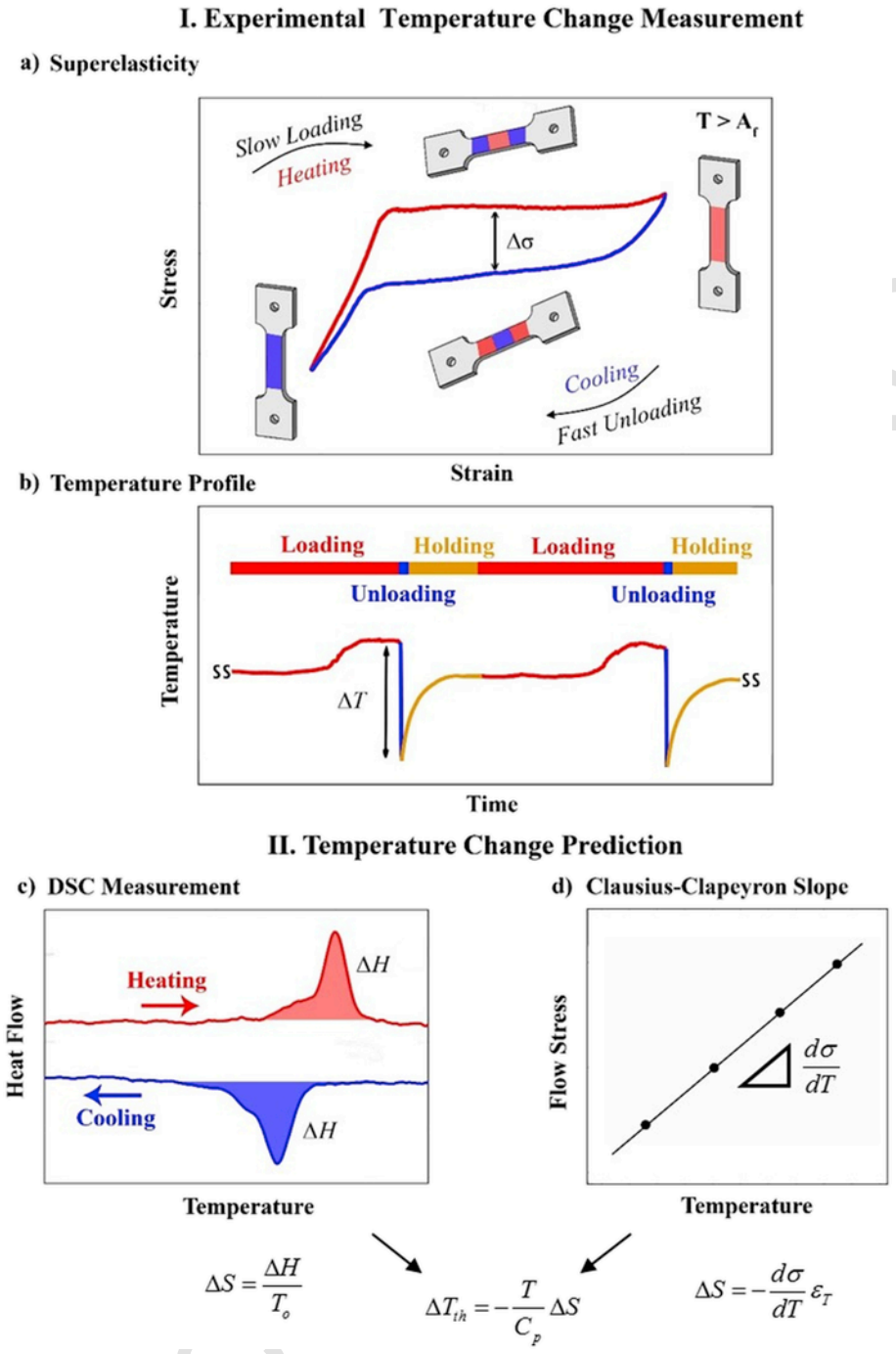

Fig. 1. A schematic that summarizes the experimental methodology and temperature change prediction for the current work. a) A schematic of the exothermic and endothermic phase transformation processes of a superelastic cycle, b) the EC cooling effect in terms of ΔT for multiple cycles, c) the DSC measurement for latent heat determination, and d) The Clausius-Clapeyron slope measured from the relationship between 0.1% offset stress and temperature.

has been illustrated with respect to the maximum applied stress, strain, and entropy change in Section 3.5. The predictions of the temperature change for each materials have been elaborated in Section 3.6.

3.1. Superelasticity of CuZnAl, Ni_2FeGa, and NiTi single crystals in tension and compression

The EC cooling effects of [001] CuZnAl, [001] Ni_2FeGa, and [148] NiTi were studied during the reverse martensitic transformation within the superelastic temperature window. As shown in Table 1, the A_f temperatures of all selected materials are close to the room temperature (25 °C). Therefore, the lower temperature limit was selected

Table 1
The nominal compositions, heat treatments, specific heat capacities, and phase transformations for the five materials are enclosed.

Material	Nominal Composition at.%	Heat Treatment	C_p J/kg K	Phase Transformation
CuZnAl	$Cu_{59.1}Zn_{27}Al_{13.8}$ with $Zr_{0.1}$	Homogenized @ 800 °C for 30min Aged @ 80 °C for 24 h A_s = 4 °C, A_f = 13 °C M_s = 1 °C, M_f = −12.5 °C	420	$L2_1$ to18R [37,38]
Ni_2FeGa	$Ni_{54}Fe_{19}Ga_{24}$	As-grown A_s = 14 °C, A_f = 22 °C M_s = 6 °C, M_f = −3 °C	460	$L2_1$ to 10M–14M to $L1_0$ at T = RT $L2_1$ to 14M to $L1_0$at T > RT [39]
$NiTiHf_{13.3}$	$Ni_{50.5}Ti_{36.2}Hf_{13.3}$	As-grown A_s = 15.2 °C, A_f = 31.5 °C M_s = −32.7 °C, M_f = −65.4 °C	570	B2 to B19' [19]
NiTiCu	$Ni_{40}Ti_{50}Cu_{10}$	Solutionized @ 920 °C for 24 h A_s = 0 °C, A_f = 31 °C M_s = −11 °C, M_f = 21 °C	560	B2 to B19' [40]
NiTi	$Ni_{50.8}Ti_{49.2}$	Solutionized @ 920 °C for 24 h Aged @ 400 °C for 1.5 h A_s = −15 °C, A_f = 0 °C M_s = −55 °C, M_f = −75 °C	590	B2 to B19' [41]

The C_p values given are approximately constant in the temperature regime from 40 °C to 80 °C for CuZnAl, Ni_2FeGa and NiTi and from 60 °C to 100 °C for NiTiCu and $NiTiHf_{13.3}$.

at 25 °C for the uniaxial tensile and compressive tests. The upper temperature limit was chosen at higher temperatures close to M_d, which is also the maximum temperature for stress-induced martensitic transformation. The applied strain of each material presented in Figs. 2 and 3 was selected to be close to the maximum transformation strain and thus the largest EC effect. The tensile stress-strain curves with a maximum strain of 10% at different temperature levels are presented in Fig. 2a and b for CuZnAl and Ni_2FeGa. As demonstrated in Fig. 2b, in the case of Ni_2FeGa, the stress hysteresis first shrinks as the temperature increases from 25 °C to 130 °C and then expands from 130 °C to 190 °C. A significant increase of hysteresis at 85 °C is evident for CuZnAl. In Fig. 2c, the stress-strain behaviors with a strain range of 4% are demonstrated from 30 °C to 75 °C for NiTi and a similar hysteresis shrinkage can also be observed within this temperature range. In general, the uniaxial tensile experiments of CuZnAl showed the lowest stress levels. It is also worthy of noting that all three materials exhibit a wide range of superelasticity with Ni_2FeGa providing the broadest interval.

In compression, we can observe a similar scenario for the evolution of stress hysteresis with increasing temperature as illustrated in Fig. 3. When compared to the tensile results in Fig. 2, the stress levels of the three materials are higher in compression. For example, in the case of Ni_2FeGa, at the same deformation temperature of 140 °C, the transformation took place at 225 MPa in tension, while at 425 MPa in compression. The strain range of CuZnAl and Ni_2FeGa decreases from 10% to 8% and 5%, respectively. In addition, the superelastic behaviors of CuZnAl were found at temperatures from 25 °C to 160 °C under compressive stress, which is a significant increase when compared to the tensile results (25 °C to 95 °C).

3.2. The evolution of temperature with time

The temperature evolution as a function of time was captured using an IR camera during a loading and unloading cycle at different deformation temperatures. The temperature of the sample was recorded by averaging the entire gauge sections and the temperature change, ΔT, was measured from the beginning of the unloading process until the sample was completely unloaded. In order to ensure the temperature changes were accurate and reproducible, they were measured during two consecutive load cycles and the results of Ni_2FeGa, CuZnAl, and NiTi are presented in Fig. 4 for both tension and compression tests. The loading process was kept at a low strain rate of 2×10^{-3} s^{-1} for CuZnAl and Ni_2FeGa and 2×10^{-4} s^{-1} for NiTi to minimize temperature rise, while a fast strain rate of 0.2 s^{-1} was applied during unloading in order to approach the adiabatic condition. A schematic of the entire experimental procedure is shown in Fig. 4g. As shown in Fig. 4a and f, the temperature profiles of the two consecutive load cycles were consistent and symmetric at different temperature levels for all three materials in both tension and compression. Especially for CuZnAl and Ni_2FeGa, such consistency extended to higher temperatures of nearly 200 °C. The slight heating was evident for all three materials during the loading process due to the exothermic forward martensitic transformation. Among all, NiTi has the most increase in temperature that is on the order of 5 °C during loading.

3.3. Evolution of phase transformation and corresponding temperature gradient with deformation

As introduced in Section 2.2, a dual camera system was set up to monitor the evolutions of both strain field and temperature gradient at different stress levels simultaneously. The comparisons between the two are presented in Figs. 5 and 6 for CuZnAl, Ni_2FeGa, and NiTi respectively at selected temperatures in tension and compression respectively. The axial DIC strain fields are illustrated on the left and the corresponding thermographs on the right. In the case of CuZnAl, the strain localization was evident upon the initiation of phase transformation (Point A in Fig. 5a). Meanwhile, a local temperature increment also took place at the same area where the local strain accumulation was observed. With further deformation, both the strain contour and temperature map became homogeneous at 10% strain and a temperature increase of approximately 1.2 °C was observed at the end of loading (Point C). At the beginning of unloading (Point D), the reverse martensitic transformation occurred at both ends of the gauge section and propagated towards the center (Point F). An immediate temperature drop of 3 °C was observed at the location where the reverse phase transformation took place at Point D. However, a higher temperature drop of 5.2 °C along the transformation zone (grey dashed line) was also evident. The higher undercooling at the transformation zone boundary can be attributed to the localized endothermic response. When the sample was fully unloaded, the ΔT was measured to be 7.02 °C. In the case of Ni_2FeGa, the reverse phase transformation took place at only one end of the gauge section and expanded to the other end. During the load process, a slight temperature increase of 1 °C was detected. Upon the completion of unloading, the ΔT was measured as 9.06 °C. In the case of NiTi, the temperature increased by 3.5 °C at the end of loading and decreased by 14.9 °C at the end of unloading. In compression, as shown in Fig. 6, a similar scenario can also be observed for the three materials.

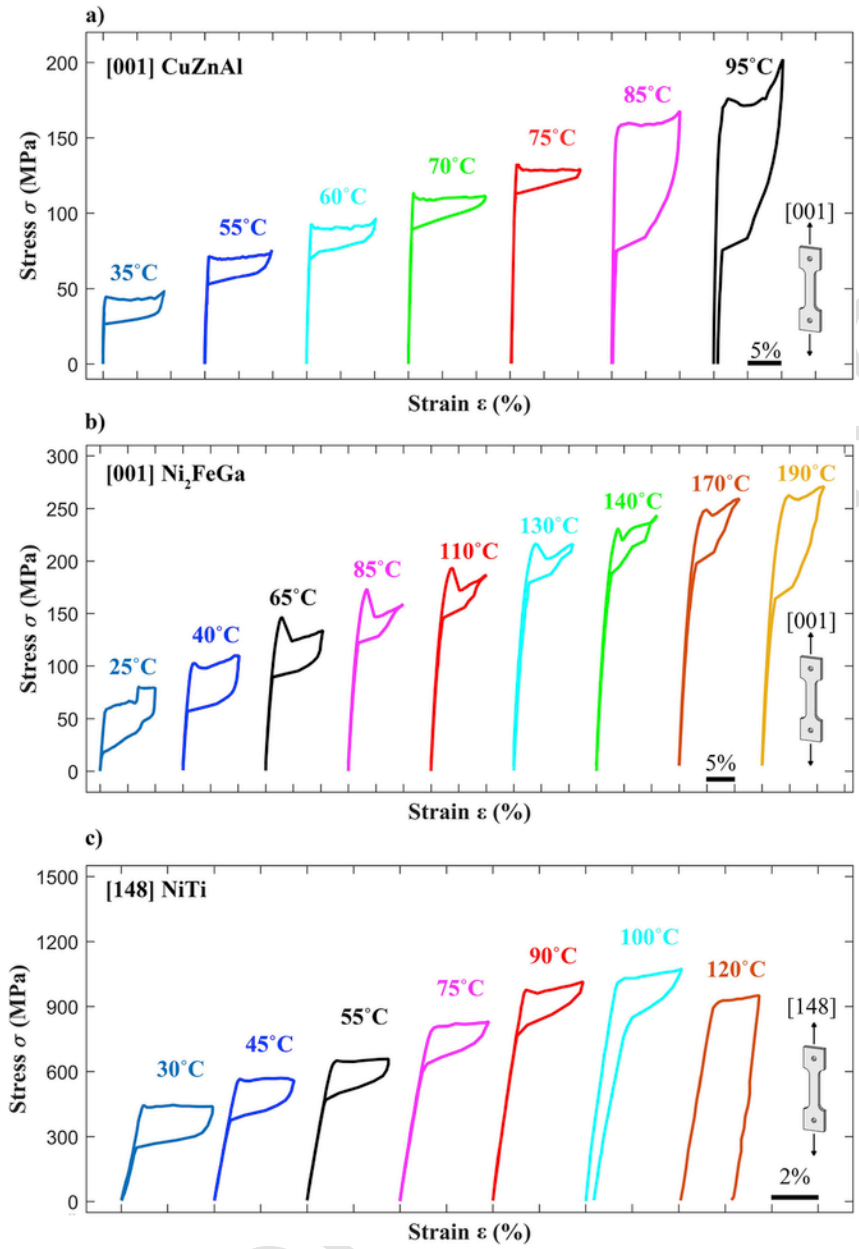

Fig. 2. The tensile stress-strain behaviors of a) [001] CuZnAl, b) [001] Ni_2FeGa, and c) [148] NiTi at different temperatures. Note that all three materials show excellent superelastic deformations at a range of temperatures.

3.4. $NiTiHf_{13.3}$ and NiTiCu single crystals – ternary addition

The additions of Hf and Cu have been considered to be the most important in NiTi-based SMAs. Fig. 7a demonstrates the stress-strain behaviors of [111] $NiTiHf_{13.3}$ at various temperature levels. The superelasticity was found in the temperature range from 5 °C to 50 °C. In this study, the EC effect of [111] $NiTiHf_{13.3}$ was measured at 45 °C. Fig. 7b shows the DIC strain contours and the corresponding temperature gradients of [111] $NiTiHf_{13.3}$ single crystal at selected load levels. The stress-strain curve with the black line was determined by averaging the axial strain fields over the entire DIC region (6 mm × 3 mm), while the blue line represented the local fields extracted from a smaller area (1 mm × 3 mm). As shown in Fig. 7b, the local transformation strain of the order of 11.8% was measured. However, the remnant strain in the order of 1.8% was irrecoverable even after heating the sample above the austenite finish temperature, A_f, confirming that the irreversibility prevailed. Due to the heterogeneous nature of the strain distribution, only a small fraction of the material in $NiTiHf_{13.3}$ underwent the austenite-to-martensite transformation. Therefore, local temperature changes in the area where large strains accumulated are expected. An obvious local temperature increment was evident upon the initiation of phase transformation at Point A. At Point B, with further deformation, the region of the local temperature increment expanded, but the overall temperature map remained heterogeneous. At the maximum strain of 14% (Point C), a slight temperature decrease was observed locally. At the completion of unloading, a local temperature drop was evident at Point E. Over-

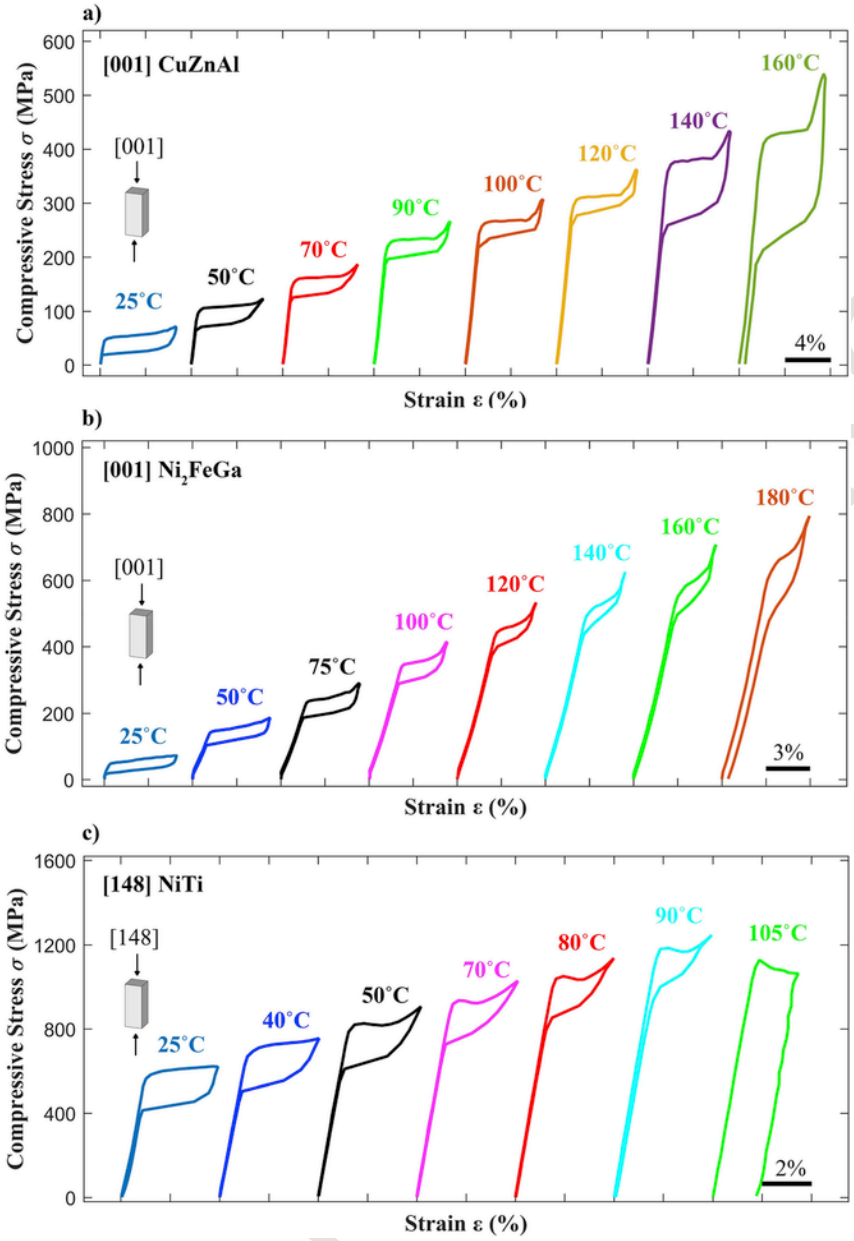

Fig. 3. Stress-strain curves of a) [001] CuZnAl, b) [001] Ni_2FeGa, and c) [148] NiTi at different temperatures in compression. Excellent superelastic behaviors were also found for the three materials.

all, the temperature of the sample first increased from 45 °C to 50 °C and then slightly decreased to 47 °C locally during loading. The local ΔT was measured to be 6.95 °C when the external load was removed adiabatically. Compared to $NiTiHf_{13.3}$, the transformation response of NiTiCu is significantly improved as shown in Fig. 8. However, the heterogeneous nature of the transformation process is still evident. The lack of reversible strains in both NiTiHf and NiTiCu also suggests their low fatigue tolerance, as such irreversibility would tend to accumulate over cycles and, therefore, deteriorate the cooling capacity of the material. One possible reason for the localization is the much larger migration stress relative to the nucleation stress. This phenomenon can be controlled by suitable heat treatments, but this is outside our scope at this time.

3.5. The effect of functional fatigue resistance on EC properties

In order to make the solid refrigerant a practical alternative to the traditional cooling solution, the good functional fatigue behavior of SMAs is the basis. The tensile fatigue response and the fatigue life, N_f, are shown in Fig. 9 for CuZnAl, Ni_2FeGa, and NiTi at chosen temperatures. The sample that didn't fail is indicated as N_f = Runout. A relatively short fatigue life, $N_f = 165$, was found for NiTi when a 4% strain range was applied (Fig. 9c). This result is also in an agreement with our previous study on NiTi [26]. All three materials exhibited consistent mechanical behaviors up to 100 cycles with small variations in the hysteresis and stress levels. In particular, Ni_2FeGa has the most stable fatigue response among all with only a small decrease in the transformation stress at 10^4th cycle.

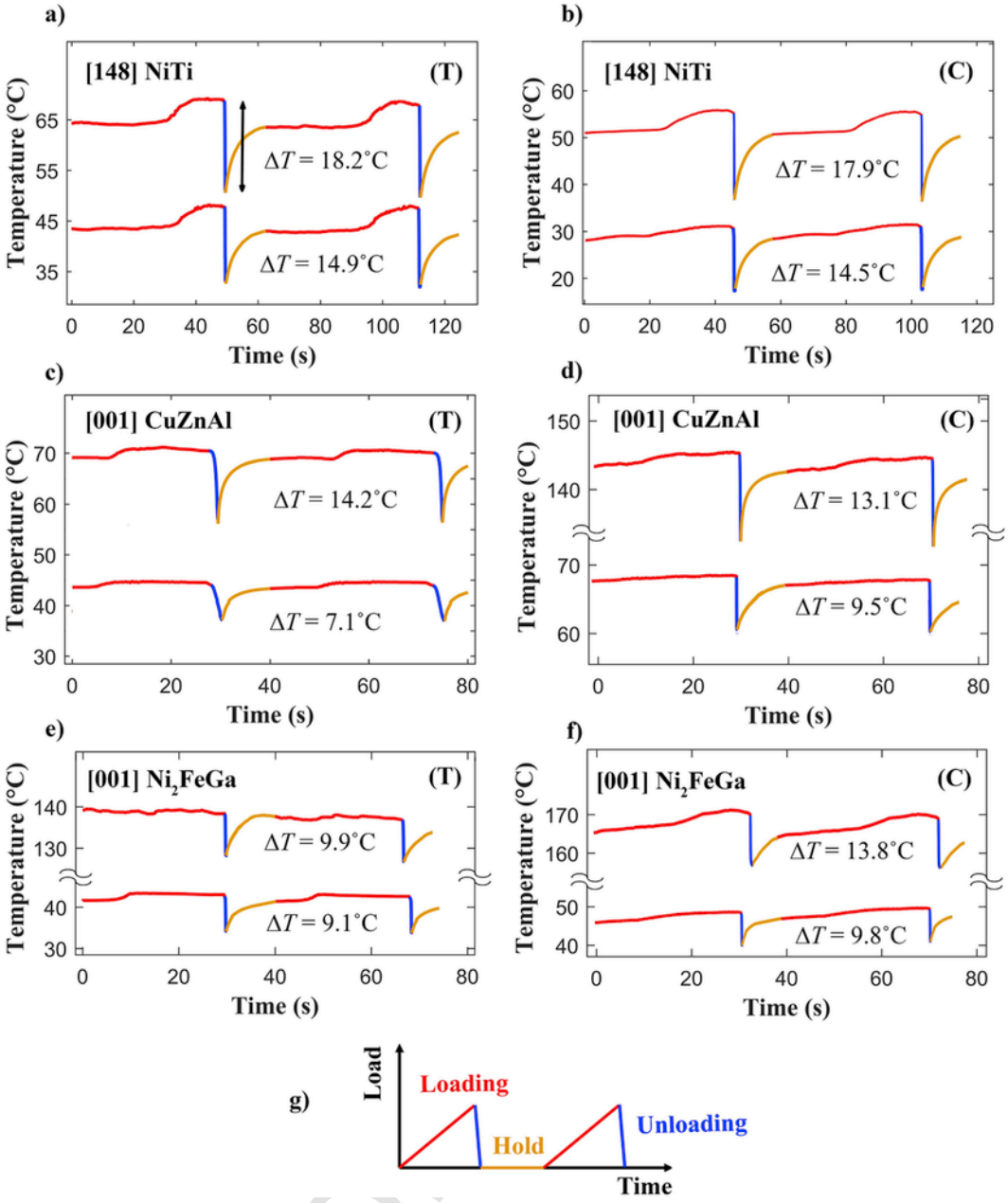

Fig. 4. Temperature drops of two consecutive load cycles at different operating temperatures are demonstrated for [148] NiTi, [001] CuZnAl, and [001] Ni_2FeGa. The temperature profiles captured during tensile experiments (T) are shown in a), c), and e) for NiTi, CuZnAl, and Ni_2FeGa, respectively. Those obtained from compressive experiments (C) are presented in b), d), and f). g) A schematic for showing the entire experimental procedures.

We also notice that studying the fatigue response of SMAs in compression has merits, as the materials will not fracture easily under compressive loading. Therefore, the mechanical behaviors upon cyclic deformation were investigated on NiTi, Ni_2FeGa, CuZnAl, and NiTiCu in compression and results are presented in Fig. 10. Remarkably, both NiTi and Ni_2FeGa exhibit superior stability to CuZnAl and NiTiCu even after 10^4 load cycles. Among all, NiTiCu has the most degradation in the stress-strain behavior under cyclic loading.

Since the EC effect has a strong correlation to the mechanical response, the material that presents superior stability in the latter over multi-cycles is also expected to show the same in the former. The degradations of the EC effects in terms of the change in ΔT were demonstrated in Fig. 11 for the selected materials in both tension and compression. On one hand, both Ni_2FeGa and NiTi show consistent ΔT upon cycling in compression, while the former also possesses the similar consistency in tension. One possible reason is that the slip resistance for Ni_2FeGa is rather high compared to its transformation stress precluding irreversibility effects [42,43]. Furthermore, CuZnAl and NiTiCu exhibit inferior fatigue endurance as shown in Figs. 9 and 10.

3.6. Temperature dependence of EC effect with respect to strain, stress and entropy levels

The effect of deformation temperature on the EC effect is illustrated in Fig. 12. The maximum temperature change, ΔT_{max}, of each

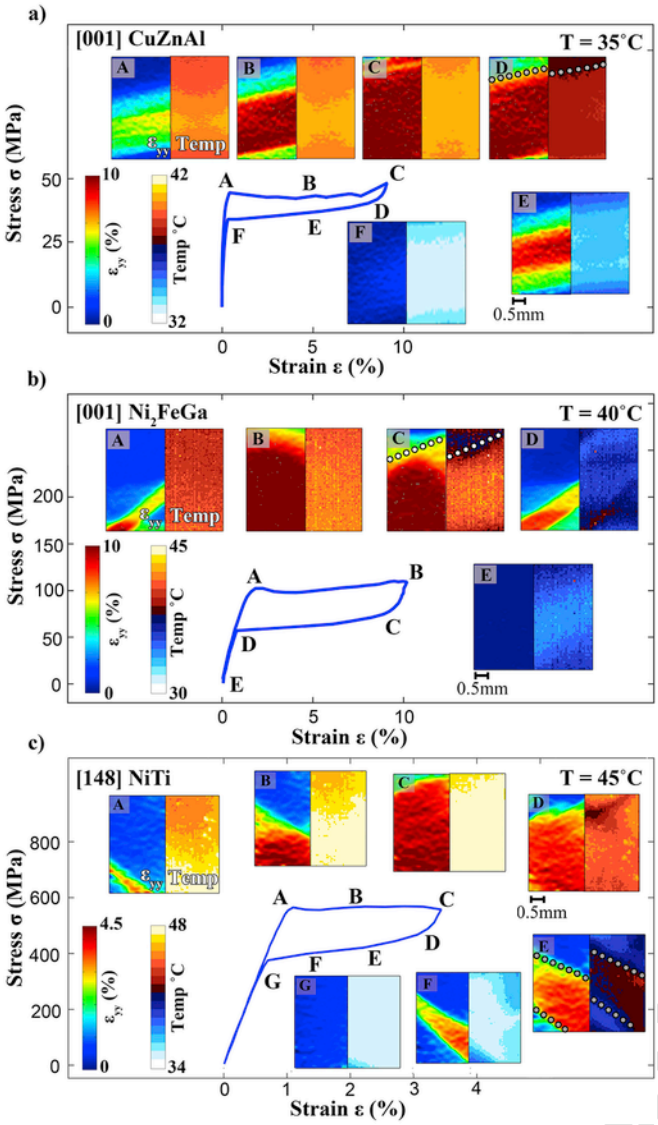

Fig. 5. A comparison between selected DIC strain field (right) and thermography (left) at different load steps for a) [001] CuZnAl at 35 °C with a localized undercooling at the transformation edge indicated at Point D as grey dashed line, b) [001] Ni_2FeGa at 40 °C with the localized undercooling at the transformation zone boundary at Point C as white dashed line, and c) [148] NiTi with the localized undercooling at the edge of the transformation zone at Point E as grey dashed line.

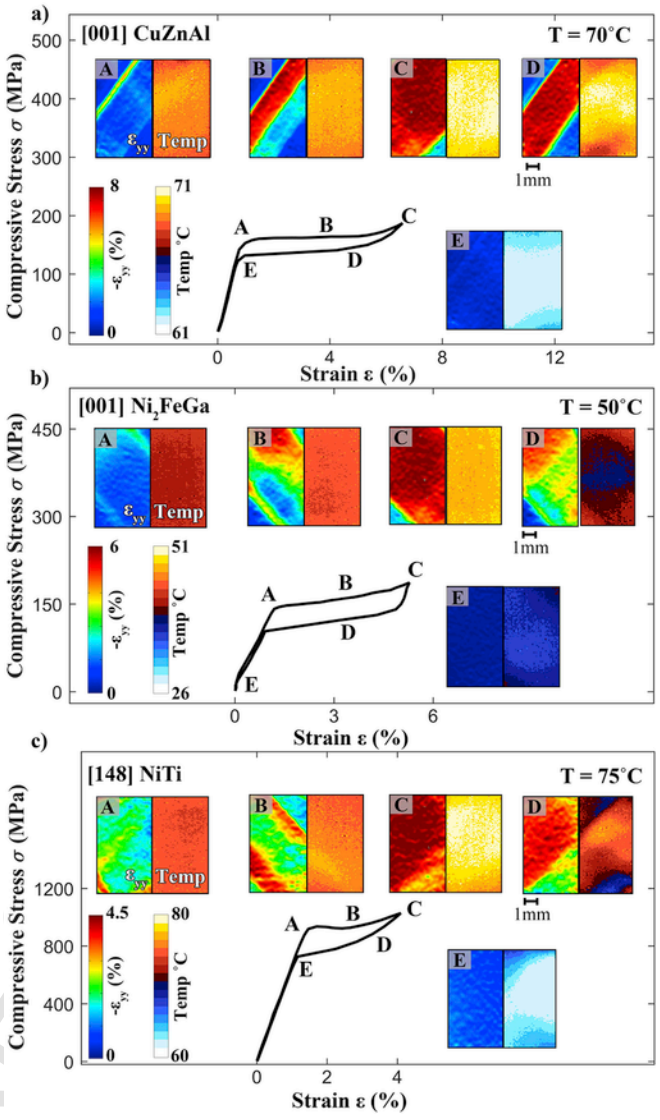

Fig. 6. A comparison between selected DIC strain field (right) and thermography (left) at different load steps for a) [001] CuZnAl at 70 °C, b) [001] Ni_2FeGa at 50 °C, and c) [148] NiTi at 75 °C in compression.

material is essentially the peak value of each curve shown in Fig. 12. The ΔT_{max} is compared to the corresponding theoretical temperature change estimated from the entropy change for each material in Section 3.7. Fig. 13a illustrates the correlation between the deformation temperature and the EC effect with respect to the maximum applied strain for each material. Overall, the ΔT_{max} were measured to be 14 °C for CuZnAl, 13.5 °C for Ni_2FeGa, 18.2 °C for NiTi, 15.2 °C for NiTiCu, and 6.95 °C for $NiTiHf_{13.3}$. Among all, Ni_2FeGa exhibits the largest temperature span of 165 °C in both loading senses extending the EC effect to high temperature regime, but the higher cooling effect can be achieved under compressive load. The CuZnAl has the largest tension and compression asymmetry particularly in terms of the temperature span. We can observe a much wider EC window that is comparable to Ni_2FeGa in compression for CuZnAl. Furthermore, a similar EC effect can be found for NiTi regardless of the stress state. In Fig. 13b, the EC performances of the materials in this study are illustrated with respect to their entropy changes. The entropy changes for each material were calculated from both the Clausius-Clapeyron slopes, ΔS^{CC}, and enthalpy change per unit volume measured from DSC, ΔS^{DSC}. In general, we observed that the material that exhibits higher entropy change will tend to have higher EC cooling capacity as well. However, as we discern later, there are other considerations that play a significant role. In Fig. 13c, the temperature dependence of EC properties is showcased in terms of applied stress levels. This figure outlines the importance of the operational stress. For example, it is evident that the applied stress of CuZnAl is much smaller than that of NiTi, which can facilitate different applications. From Figs. 12 and 13, it is evident that the ΔT increases initially and then decreases with further temperature increase. The underlying mechanism can be related to the variation of hysteresis with accruing deformation temperature, which will be elaborated in the discussion section.

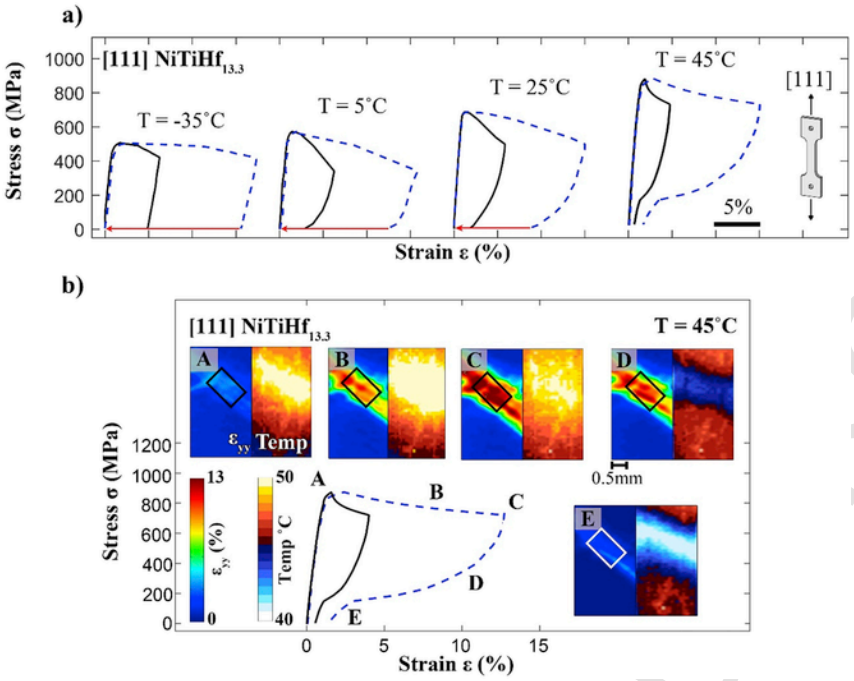

Fig. 7. a) The stress-strain behavior of [111] $NiTiHf_{13.3}$ at selected temperatures. The solid black line indicates the overall stress-strain behavior, while the blue dashed line represents the local behavior extracted from the rectangular region on the DIC strain contour shown in part b). b) The comparisons between DIC strain field and thermography at selected load steps are demonstrated for $NiTiHf_{13.3}$ at 45 °C. (For interpretation of the references to colour in this figure legend, the reader is referred to the web version of this article.)

3.7. Temperature change estimation from entropy changes

During the experiments, the measured ΔT does not necessarily represent the real adiabatic temperature change. To evaluate the maximum achievable temperature change, ΔT_{th}, we used the entropy change per unit mass, ΔS, calculated from both the Clausius-Clapeyron slopes (Method I) and enthalpy change per unit volume, ΔH (Method II).

The flow stresses were extracted from the stress-strain behaviors shown in Fig. 14 with 0.1% offset. The flow stress corresponds to the critical stress of the forward phase transformation (σ_F). The linear relationships between flow stresses and temperatures are presented in Fig. 14 for CuZnAl, Ni_2FeGa and $NiTiHf_{13.3}$. Note that the Clausius-Clapeyron slopes based on the forward transformation stresses, $\frac{d\sigma_F}{dT}$, were found to be 2.01 MPa/°C for CuZnAl, 0.99 MPa/°C for Ni_2FeGa, 5.1 MPa/°C for $NiTiHf_{13.3}$, and 7.02 MPa/°C for NiTi in tension. Under compressive loading, the slopes were found to be 2.87 MPa/°C for CuZnAl, 3.78 MPa/°C for Ni_2FeGa, 8.82 MPa/°C for NiTi, and 5.17 MPa/°C for NiTiCu. The asymmetry in the overall transformation stress can also be perceived from the correlation between stress and temperature in Fig. 14, where the elevation of tensile stresses as the temperature increases is rather slow as opposed to the compressive stresses. This is mainly due to the asymmetry in tension and compression transformation strains affecting the slopes. The slopes of the reverse transformation stress (σ_R) and the equilibrium stress (σ_E) were also measured for the selected materials, where σ_E is defined as the average of σ_R and σ_F. We note that the resulting slopes are close in all three cases and the difference between slopes is below 2.4%.

The latent heat ΔH can be extracted from the DSC results by averaging the areas under the heat flow vs. temperature curves. The DSC results of CuZnAl, Ni_2FeGa, $NiTiHf_{13.3}$, NiTi, and NiTiCu are presented in Fig. 15 with the transformation temperatures labeled in the graphic. The latent heats ΔH were measured to be 6.69 J/g for CuZnAl, 5.67 J/g for Ni_2FeGa, 15.9 J/g for $NiTiHf_{13.3}$, 12.7 J/g for NiTi, and 11.3 J/g for NiTiCu.

With both slopes (Method I) and ΔH (Method II) determined, ΔS can be calculated using Clausius-Clapeyron relationship given in Equation (1),

$$-\Delta S = \frac{d\sigma}{dT}\varepsilon_T = -\frac{\Delta H}{T_o} \tag{1}$$

where ε_r is the transformation strain and T_0 is the thermodynamic equilibrium temperature between austenite and martensite, and ΔH is the enthalpy of the transformation per unit mass. We note that in a recent paper published by Niitsu et al. [44] the entropy change was determined by the peak temperature, T_p, corresponding to the reverse martensitic transformation (M to A). The ΔS calculations using both T_o and T_p are included in this study as well. The transformation strain for each material was calculated using Lattice Deformation Theory (LDT) [45]. A reasonable approximation for calculating T_0 was provided by Tong and Wayman in Equation (2) [46].

$$T_o = \frac{1}{2}\left(M_s + A_f\right) \tag{2}$$

ΔT_{th} can be estimated via Equation (3) assuming fully adiabatic condition,

$$\Delta T_{th} = -\frac{T}{C_p}\Delta S \tag{3}$$

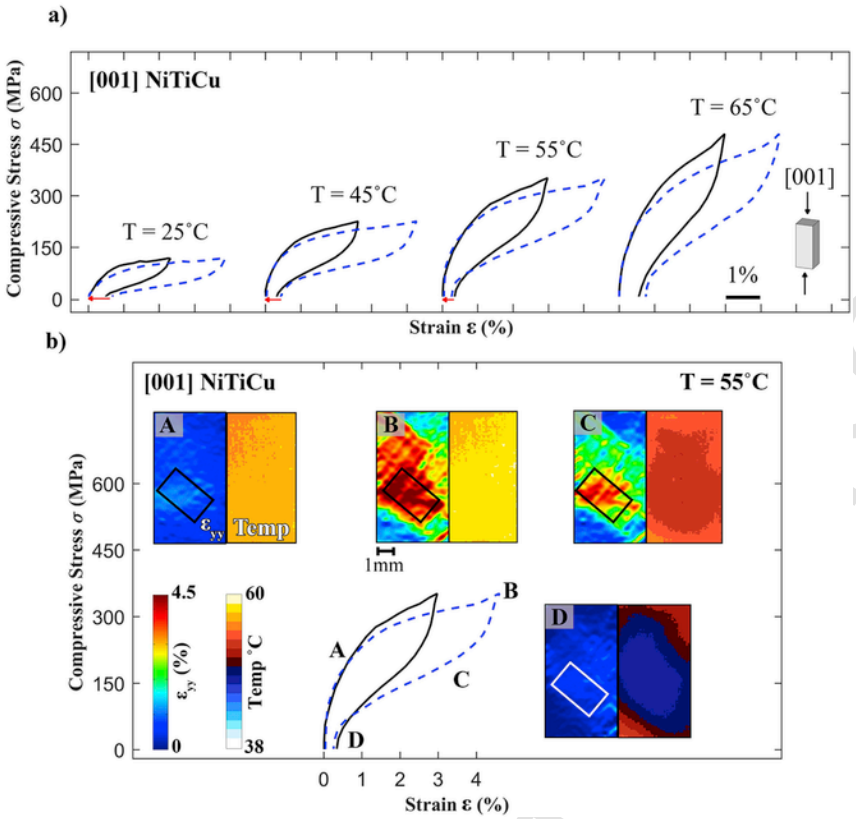

Fig. 8. a) The stress-strain behavior of [001] NiTiCu at selected temperatures. The solid black line indicates the overall stress-strain behavior, while the blue dashed line represents the local behavior extracted from the rectangular region on the DIC strain contour shown in part b). b) The comparisons between DIC strain fields and thermographies at selected load steps are demonstrated for NiTiCu at 55 °C. (For interpretation of the references to colour in this figure legend, the reader is referred to the web version of this article.)

where T is the test temperature at which ΔT_{max} was measured experimentally (see Fig. 12), ΔS was calculated from Equation (1), and C_p is the specific heat of each material given in Section 2.1. The ΔS was determined from the Clausius-Clapeypron relationship that involves $\frac{d\sigma}{dT}$ and ε_T. The $\frac{d\sigma}{dT}$ is essentially constant as shown in Fig. 14 and the ε_T is the theoretical transformation strain. Therefore, the entropy change is fairly constant within the superelastic temperature window from A_f to M_d. In this study, the C_p values given are approximately constant in the temperature regime from 40 °C to 80 °C for CuZnAl, Ni_2FeGa and NiTi and from 60 °C to 100 °C for NiTiCu and $NiTiHf_{13.3}$. According to the ASTM standard E1249, the C_p values of CuZnAl, Ni_2FeGa, NiTi, NiTiCu, and $NiTiHf_{13.3}$ were obtained as 420, 460, 590, 560, and 570 J/kg K respectively as shown in Table 1. The ΔT_{th} of each material was estimated using these C_p values via Equation (3).

The calculated ΔS and ΔT_{th} from both Method I (tension and compression) and Method II are tabulated in Tables 2–4 respectively. Note that the difference between $\frac{d\sigma_F}{dT}$ and $\frac{d\sigma_E}{dT}$ of each case is below 2.4%. In Tables 2 and 3, the ΔS and ΔT_{th} were calculated using $\frac{d\sigma_E}{dT}$. As expected, the NiTi-based SMAs have the highest ΔS among the five materials. Although CuZnAl and Ni_2FeGa have lower ΔS values, they are still able to yield sufficient ΔT_{th} in the order of 16.9 °C and 12.8 °C, respectively. A comparison between the ΔT_{th} and ΔT_{max} measured from experiments are included as well. In general, the ΔT measured from the experiments falls short of the ΔT_{th} determined from ΔS for all cases. Further rationalization can be found in the discussion section. Note that the temperature changes, ΔT_{th} and ΔT_{th}^{Tp}, evaluated from T_o and T_p respectively are close as shown in Table 4.

In the case of Ni_2FeGa, the inter-martensitic transformation ($L2_1 \leftrightarrow 14M \leftrightarrow L1_o$) [47] [48] can take place over the single stress plateau of the superelastic curves shown in Figs. 2b and 3b. Since the entropy change (ΔS) is independent of path and only depends on the initial and final states of the phase transformation [49], the ΔS associated with $L2_1 \leftrightarrow 14M \leftrightarrow L1_o$ can be obtained from the ΔS of $L2_1 \leftrightarrow L1_o$. The entropy change calculation based on the $\frac{d\sigma}{dT}$ and ε_T values reported by Sutou et al. [47] shows that $\Delta S(L2_1 \rightarrow 14M)$ is −12.5 J/kg K, $\Delta S(14M \rightarrow L1_o)$ is 0.67 J/kg K, and $\Delta S(L2_1 \rightarrow L1_o)$ is −13.3 J/kg K. Note that $\Delta S(L2_1 \rightarrow 14M) + \Delta S(14M \rightarrow L1_o) = \Delta S(L2_1 \rightarrow L1_o)$. This value of −13.3 J/kg K is also in agreement with our entropy calculation for Ni_2FeGa (−14.6 J/kg K). In addition, the $\frac{d\sigma_E}{dT}$ (on the order of 1.01 MPa/K) of Ni_2FeGa measured in this study is very close to that of $L2_1 \rightarrow L1_o$ (1.12 MPa/K) reported by Sutou et al. [47]. Therefore, we use the ΔS corresponding to $L2_1 \rightarrow L1_o$ transformation for Ni_2FeGa in this study.

4. Discussion of results

4.1. Tension-compression asymmetry

The asymmetric deformation behaviors of tension and compression can be clearly noted for NiTi, CuZnAl, and Ni_2FeGa in Figs. 2 and 3. The observed tension/compression asymmetry can be ascribed to the unidirectional nature of the shear strain across the transforma-

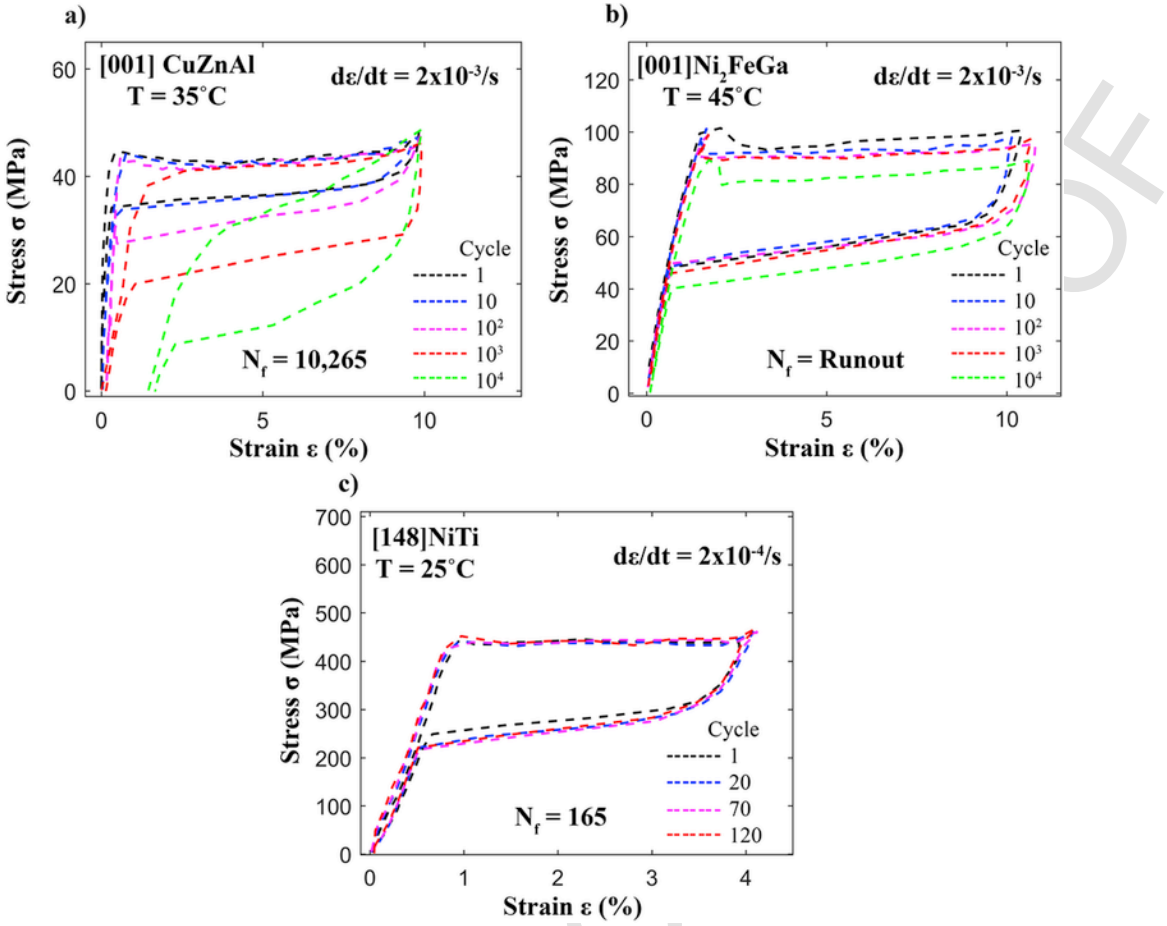

Fig. 9. The tensile functional fatigue responses of a) [001] CuZnAl, b) [001] Ni_2FeGa at a strain rate of 2×10^{-3} s^{-1} with a strain range of 10%, and c) NiTi at a strain rate of 2×10^{-4} s^{-1} with a strain range of 4%.

tion habit planes [50]. If the phase transition is triggered by the resolved shear stress in a prescribed transformation direction, the similar process will not occur in the opposite direction [51]. In this regard, the phase transformation will be nucleated in different sets of crystallographic plane and direction for tension and compression respectively. Since the stress levels, hysteresis, and temperature intervals of the superelastic loops vary between tension and compression, they also translate to different EC performances as demonstrated in Fig. 12.

4.2. The role of inhomogeneity of phase transformation on EC response

The effect of inhomogeneous phase transformation on the EC properties of SMAs was investigated in this study. In Fig. 16, the transformation inhomogeneity is quantified for each material in terms of strain histograms that were constructed from the DIC strain contours illustrated from Figs. 5–8. In the cases of NiTi, Ni_2FeGa, and CuZnAl, the strain distributions across the materials are uniform as the widths of their strain histograms are small. On one hand, we noted that the Hf-alloyed samples have the largest strain variations across the material, which also indicates a highly heterogeneous nature of phase transition. In this case, the measured adiabatic ΔT is 6.95 °C, which falls far shorter than those of other materials. On the other hand, the strain distribution in the case of NiTiCu ternary alloys is less heterogeneous (reduced width) than NiTiHf and the ΔT is measured as high as 15 °C. Nevertheless, it is not expected that this value can be reproducible upon successive loading cycles. Indeed, the cooling capacity of NiTiCu degrades much more rapidly than those of the others after the first 100 cycles (Fig. 11). Therefore, to enhance the efficacy of the EC performance of SMAs, the homogeneous phase transformation process is preferred.

4.3. The role of cyclic loading on the EC properties of SMAs

As elucidated in Figs. 9–11, a strong effect of long-term cyclic deformation (in excess of 10^4 cycles) on the corresponding EC effects can be appreciable for the selected materials. Note that the EC responses of NiTi and Ni_2FeGa (Fig. 11) showed excellent reproducibility after multiple cycles of loading and unloading as an outcome of the stable superelastic loops. However, the fatigue life of NiTi falls far shorter than those of CuZnAl and Ni_2FeGa under tensile loading as depicted in Fig. 9. The reason for the early failure of NiTi is very complicated and could be related to the large particles, i.e. carbides, in the material matrix that facilitate rapid crack propagation [26,52]. The fatigue lives however improve considerably in the case of compression. We also note that the results correspond to [148] orientation, and the [111] orientation is expected to perform better. The choice of [148] was to maintain the same orientation between tension and compression where in compression the [148] exhibits the highest strains.

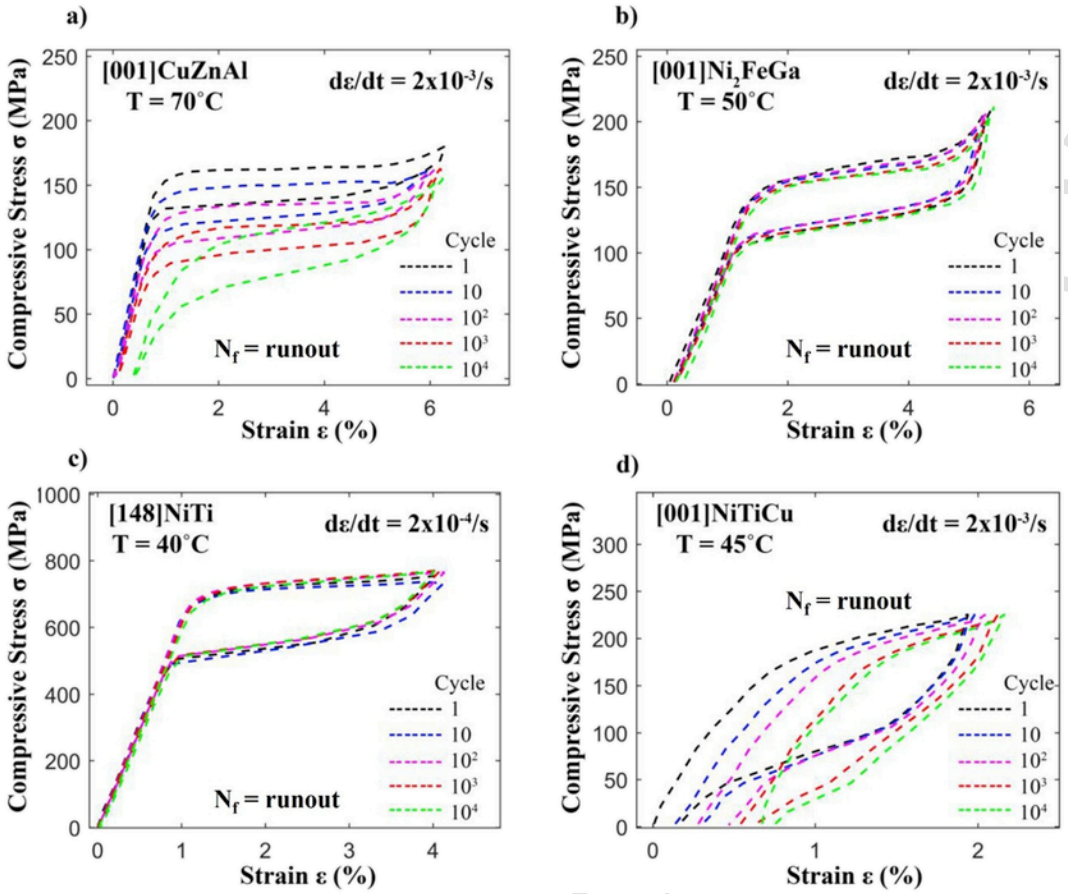

Fig. 10. The compressive functional fatigue responses of a) [001] CuZnAl, b) [001] Ni_2FeGa at a strain rate of 2×10^{-3} s^{-1} with a strain range of 6%, c) NiTi at a strain rate of 2×10^{-4} s^{-1} with a strain range of 4%, and d) NiTiCu at a strain rate of 2×10^{-3} s^{-1} with a strain range of 2%.

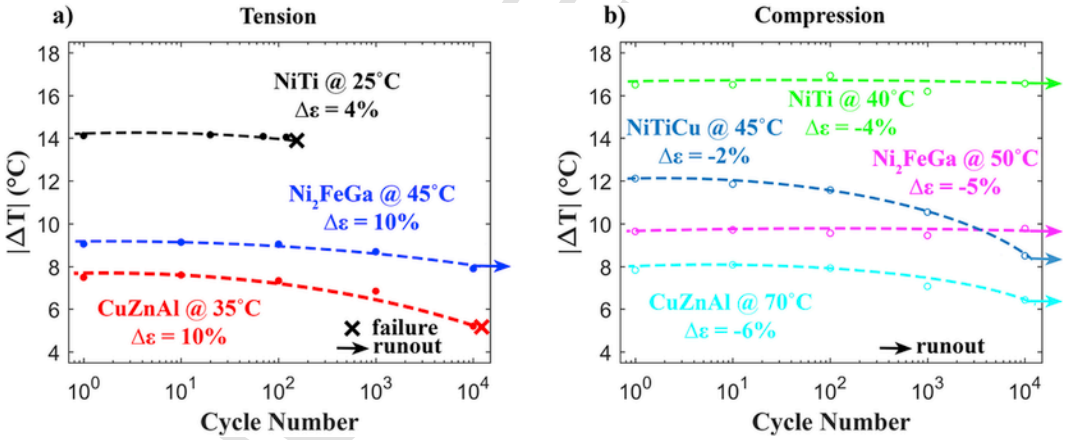

Fig. 11. The EC fatigue of the materials when deformed in a) tension and b) compression.

4.4. The role of stress hysteresis on EC properties of SMAs

In Fig. 12, we note that, for most cases, the elastocaloric effects, in terms of ΔT, first amplify and then attenuate with increasing test temperature, T. This trend has been reported in earlier literature as well [6,31]. We may seek ramifications for this phenomenon from the mechanical response that is intrinsically connected with the EC effect. As demonstrated in Fig. 17, the correlation between stress hysteresis, $\Delta\sigma$, and ΔT as a function of T is illustrated. The former represents the difference between upper and lower stress plateau as shown in the superelastic loops (Figs. 2 and 3). From Fig. 17, an inverse relationship between $\Delta\sigma$ and ΔT can be readily observed, where the maximum in ΔT corresponds well to the minimum in $\Delta\sigma$. It is evident that $\Delta\sigma$ shrinks with increasing T initially for all three cases. This trend has been discussed in early works and the interplay between

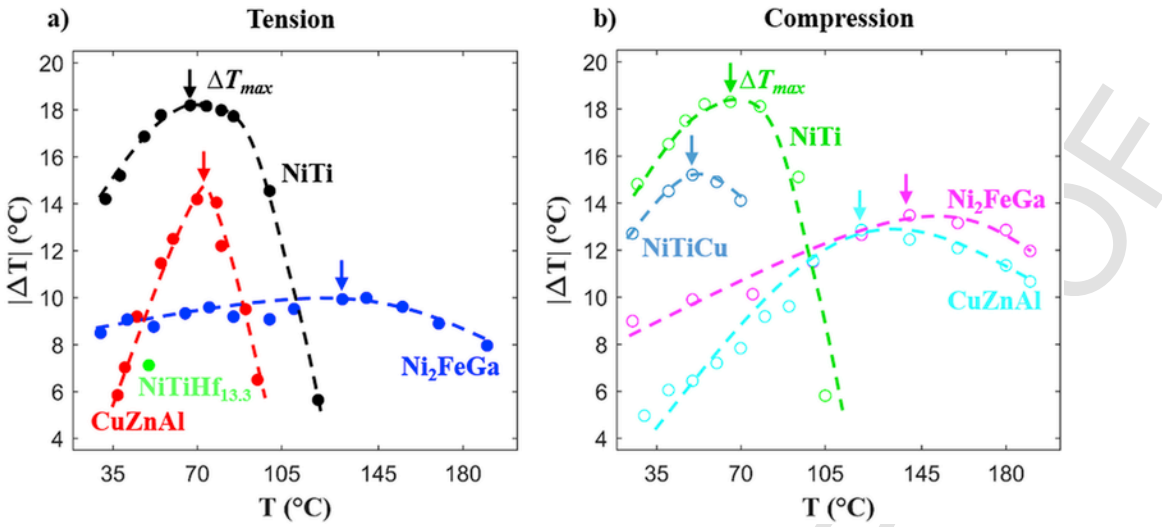

Fig. 12. The measured temperature change, ΔT, as a function of test temperatures a) in tension and b) in compression. The peak value of each curve is denoted as ΔT_{max}.

plastic dissipation and transformation play a role in NiTi (Ni = 50.8 at.%) and Ni_2FeGa [14,53,54]. The results on NiTiCu follow similar trends to those of NiTi and Ni_2FeGa. Increase in resistance to elastic strain energy dissipation would result in lower stress hysteresis. With further T increase, the energy dissipation due to the plastic relaxation effect becomes more profound [15]. This may produce a substantial $\Delta\sigma$ growth and ΔT decrease. More details regarding the variation of $\Delta\sigma$ with T have been discussed in depth by Hamilton et al. [14].

The energy dissipation in the form of frictional work gives rise to the stress hysteresis [14]. Such hysteretic loss can be characterized by the hysteresis area of the stress-strain curve. The corresponding irreversible temperature change, ΔT_{irr}, can be evaluated as follows: $\Delta T_{irr} = \frac{1}{\rho C_p}\oint \sigma \cdot d\varepsilon$ [5,55], where the integral corresponds to the area inside the σ-ε loop and ρ is the density. We evaluated the integral for the experiment that produces the maximum temperature change for each material. In this paper, ΔT_{irr} are calculated for CuZnAl, Ni_2FeGa, and NiTi. The densities of CuZnAl, Ni_2FeGa, and NiTi are 7700 kg/m^3, 8450 kg/m^3, and 7600 kg/m^3 respectively [9]. The specific heat capacities, C_p, are listed in Table 1 for each material. The ΔT_{irr} of CuZnAl is calculated as 0.77 °C and 0.96 °C for tension and compression respectively. In the case of Ni_2FeGa, the ΔT_{irr} is 0.93 °C in tension and 0.54 °C in compression. In the case of NiTi, the ΔT_{irr} is 1.52 °C in tension and 1.18 °C in compression. In summary, for optimal EC properties of SMAs, the investigation should be performed at a temperature where the hysteresis is the lowest as the energy dissipation can be minimized. Most previous works have not explored the optimal temperature, and were mostly confined to RT experiments.

4.5. The role of entropy changes on the EC response

The ΔT_{th} of each material has been determined from the ΔS that was obtained from $\frac{d\sigma}{dt}$ (Method I) and ΔH (Method II) as shown in Tables 2, 3, and 4. Note that we have acquired similar ΔS regardless of the load states (tension and compression). However, the difference between theoretically determined ΔT_{th} and experimentally measured ΔT is evident. When comparing ΔT_{th} to ΔT, a substantial difference of more than 50% can be observed in the case of $NiTiHf_{13.3}$. This can be attributed to the significant hysteretic losses resulting from the incomplete phase transformation and the plastic deformation in the local region (Fig. 7b). Since the major fractions of the material remain untransformed, this can create a highly inhomogeneous temperature profile [24], which can further reduce the cooling efficiency. In addition, the plastic deformation in the local region jeopardizes the reverse martensitic transformation and thereby leading to small ΔT. Even though similar discrepancy between ΔT_{th} and ΔT is still evident for NiTi and NiTiCu, the difference is significantly reduced. In the cases of CuZnAl and Ni_2FeGa, the magnitudes of ΔT_{th} are close to the experimentally measured ΔT. However, in the previous study, a difference of 50% between ΔT and ΔT_{th} was reported for polycrystalline CuZnAl [6]. In the current study, a better agreement was achieved in [001] CuZnAl single crystal. One plausible explanation is that the phase transformation process of polycrystalline materials may result in higher levels of dissipation (hysteresis) [19] but this difference needs to be better understood in the future.

From the experimental measurements, the local transformation strains for CuZnAl, Ni_2FeGa, and NiTi were 10% and 8%, 12.5% and 6%, and 6.2% and 6% under tension and compression respectively. We note that these measured local strains are all very close to the corresponding theoretical values listed in Tables 2 and 3 for each material. The only exceptions are the tensile strains for Ni_2FeGa and NiTi which resulted in 12.5% and 6.2% respectively-the theoretical values are 14.5% and 7.5% respectively. The resulting entropy change of Ni_2FeGa calculated using the measured transformation strain (12.5%) and Equation (1) is 12.4 J/kg K. This value of 12.4 J/kg K is about 13% smaller than the ΔS^{CC} of 14.6 J/kg K reported for Ni_2FeGa in Table 2. The corresponding temperature change of Ni_2FeGa calculated from this entropy change of 12.4 J/kg K is 10.9 K, which is closer to the experimental ΔT_{max} of 10.1 K. In the case of NiTi, the entropy change calculated using the local experimental strain (6.2%) is 43.6 J/kg K compared to the ΔS^{CC} of 52.7 J/kg K reported in Table 2. The resulting temperature change of NiTi estimated using 43.6 J/kg K is 25 K. This value of 25 K is lower than the ΔT_{th} = 30.2 K reported in Table 2 and both values exceed the experimental level of ΔT_{max} = 18.2 K. The experimental techniques of strain measurement may not reach the resolution required to capture the true transformation strains at the variant level. However, considering that individual martensite variants must undergo the Bain (intrinsic shear) strain at the local level [56], the theoretical transformation strain (which is very close to the experimental value in most cases) is chosen for the

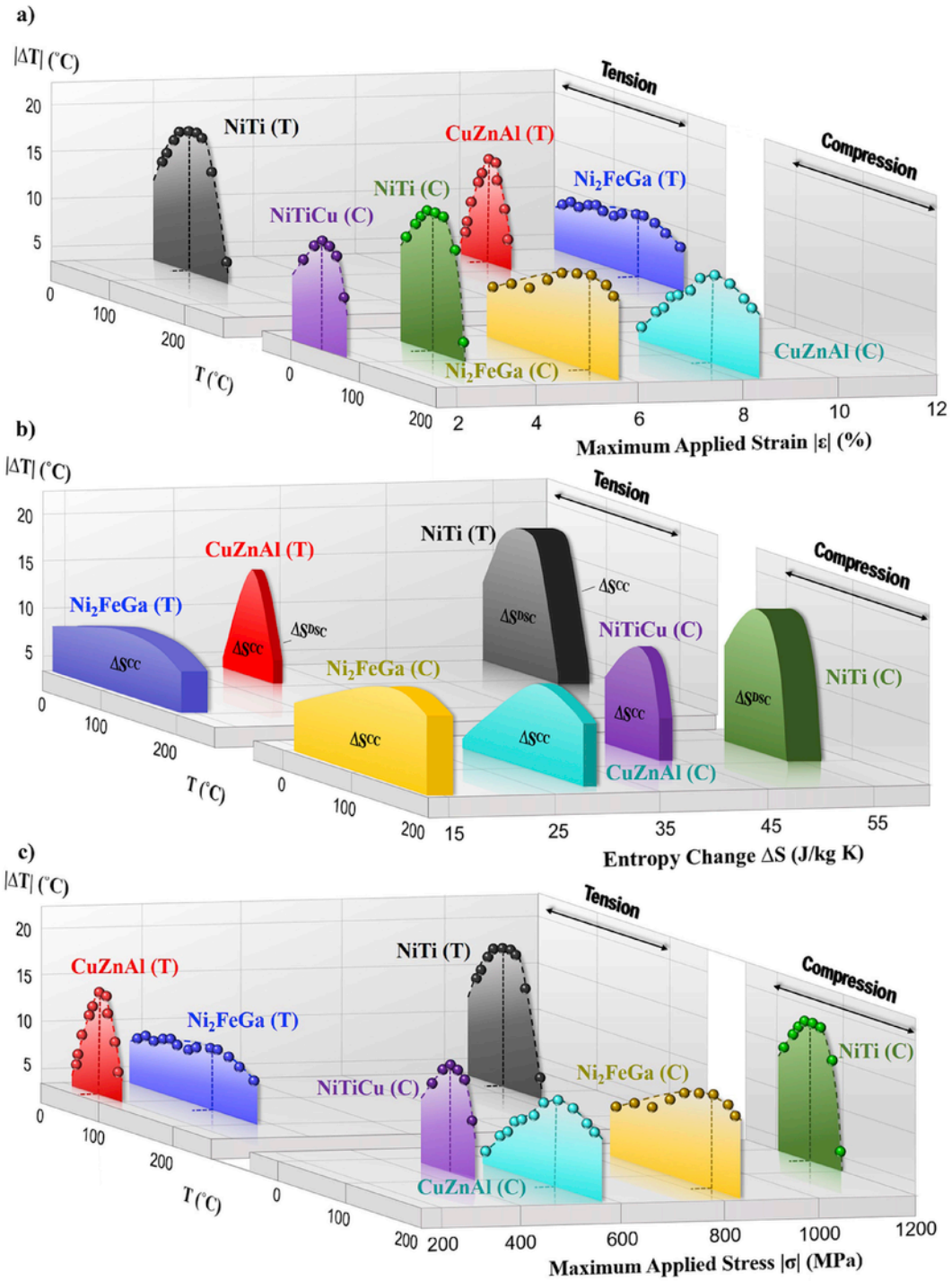

Fig. 13. a) The adiabatic temperature changes as a function of temperatures for the EC effect of CuZnAl, Ni_2FeGa, NiTi, and NiTiCu SMAs in this study were showcased in this plot. The lines are added between the data points in order to aid the eyes. The temperature spans were highlighted for each material underneath the data points. The maximum ΔT and the temperature at which maximum ΔT was found are marked with the dashed line for each material. b) The temperature dependence of the EC effects for the selected materials were manifested with respect to their entropy change determined from Clausius-Clapeyron slopes, ΔS^{CC}, and DSC analysis, ΔS^{DSC}. For Ni_2FeGa, CuZnAl, NiTiCu the magnitude of ΔS^{CC} is smaller than ΔS^{DSC}. However, the former is greater than the latter in the case of NiTi. The thickness represents the difference between ΔS^{CC} and ΔS^{DSC}. Details about the entropy change calculation were included in this paper as well. c) The temperature dependency for the EC effects of the selected materials were manifested with respect to their maximum applied stress.

entropy calculation. This choice is also consistent with our previous treatment [11].

A higher ΔS is required for better EC cooling performance (Fig. 12). In the case of NiTi-based SMAs, a recent paper showed that the entropy change displays complex dependence on Ni content (50 at.% to 51.8 at.%) in binary NiTi alloys [44]. The general trend shows that ΔS decreases with increasing Ni content. From the perspective of ΔS solely, the material with low Ni content will be more promising for

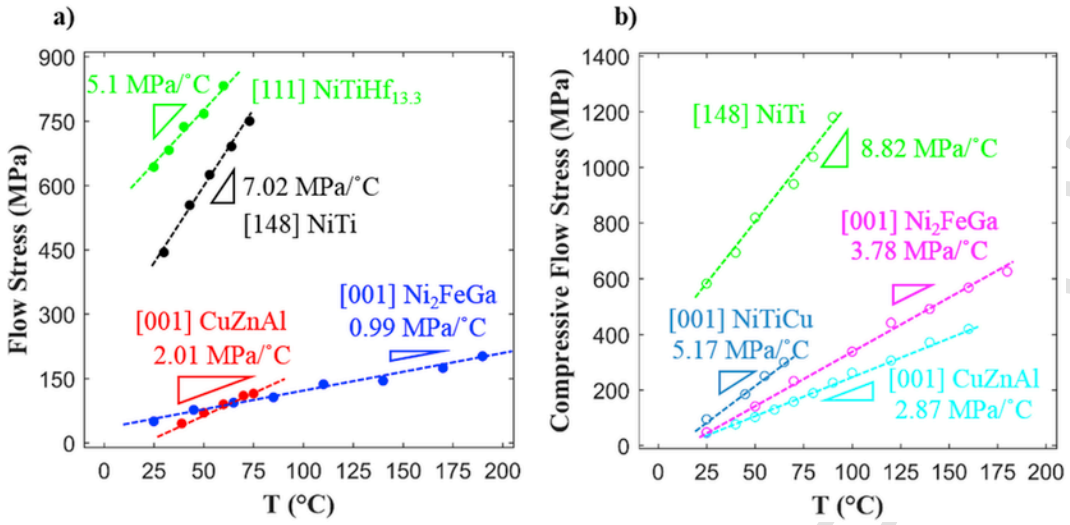

Fig. 14. Flow stresses as a function of temperatures for [001] CuZnAl, [001] Ni_2FeGa, [111] $NiTiHf_{13.3}$, [148] NiTi, and [001] NiTiCu in a) tension and b) compression. The Clausius-Clapeyron slopes are marked on the figure for all five materials.

EC application. In fact, when the Ni content is lower than 50.7 at.%, the superelastic deformation becomes harder to realize [57]. However, as the Ni content increases, the superelastic response and fatigue life will also be curtailed due to the loss of ductility. Therefore, Ni rich compositions in the vicinity of 50.5 at.% to 50.8 at.% Ni provide a good compromise. Similarly, the comparison between $NiTiHf_{13.3}$ and the other four SMAs has been exemplified in this work to elucidate the fact that an adequate balance between superelastic behaviors and ΔS needs to be achieved in order to induce an optimal EC strength. Even though $NiTiHf_{13.3}$ exhibits the highest entropy change, it is underperforming compared to others. Therefore, the magnitude of entropy change does not solely guarantee the efficacy of EC cooling, i.e. the mechanical response is also a crucial factor.

4.6. Summary of the discussion in capsule form

In summary, the current work uncovered the effect of i) the deformation temperature, ii) the stress hysteresis, iii) the inhomogeneity of transformation, and iv) the long-term cycling on the EC effect (the adiabatic temperature change) of SMAs. As the temperature increases, the temperature change capabilities of SMAs can be optimized when the stress hysteresis (i.e. energy dissipation) is minimized. In addition, we draw attention to the need for a spatially homogeneous phase transformation behavior as studied here. As an example of the $NiTiHf_{13.3}$ SMAs, the phase transformation zones remain localized with large untransforming domains. The accumulation of the remnant strain in the local region limits their strain reversibility. Therefore, when compared to the other four materials, the $NiTiHf_{13.3}$ SMAs have the lowest adiabatic temperature change despite also having the highest entropy changes. Furthermore, the functional degradation was evident upon cyclic loading for all materials in tension. In compression, the giant caloric effects were sustained in the case of NiTi and Ni_2FeGa even after 10^4 cycles. Overall, the work underscores the need for a multifaceted approach combining the determination of entropy changes (via multiple techniques) in order to predict the maximum temperature change capacities of a material, the evaluation of the stability of the thermal performance associated with functional fatigue responses under multi-cycles, and at different temperatures. Such an approach can be exploited as a guidance for future EC research on SMAs.

5. Conclusions

In this study, the EC effects of CuZnAl, Ni_2FeGa, $NiTiHf_{13.3}$, NiTiCu, and NiTi single crystals were investigated. We draw the following conclusions based on the results:

1. The mechanical behavior plays an important role in the elastocaloric performance of SMAs. The small hysteresis, less strain heterogeneity, and exceptional fatigue resistance are desired features as they optimize the elastocaloric response by limiting energy dissipation and improving reversibility.
2. The correlations between stress hysteresis and cooling capability as a function of deformation temperatures have been revealed in the current study for CuZnAl, Ni_2FeGa, and NiTi. An inverse relationship between the two has been uncovered. It was found that the cooling capacity of a SMA can be optimized corresponding to minimal hysteresis.
3. The Ni_2FeGa single crystals have the largest temperature span of 165 °C among the selected SMAs in this study. The experimentally measured ΔT in the order of 8–13 °C has been demonstrated at high temperature regimes close to 200 °C. The Ni_2FeGa performs better than other alloys in tension in view of its fatigue resistance exceeding 10^6 cycles (only 10^4 shown) for a strain of 10%.
4. A strong effect of long-term cycling (in excess of 10^4 cycles) has been uncovered in both tension and compression. Functional degradation is evident for all materials in tension. However, NiTi and Ni_2FeGa showed excellent reversibility and reproducibility of elastocaloric strength (ΔT) in compression even after 10^4 cycles.
5. In all cases, the adiabatic temperature changes determined from direct experimental measurements fall shorter than those estimated from ΔS. Such difference is expected as the energy dissipation (i.e. hysteresis) during phase transformation is inevitable. In addition, the transformation heterogeneity, especially in the case of $NiTiHf_{13.3}$, can also reduce the efficacy of the elastocaloric effect, which can be another plausible explanation for the discrepancy.

Acknowledgement

The work is supported by the National Science Foundation, DMREF grant # 1437106. The EBSD analysis was carried out in part in

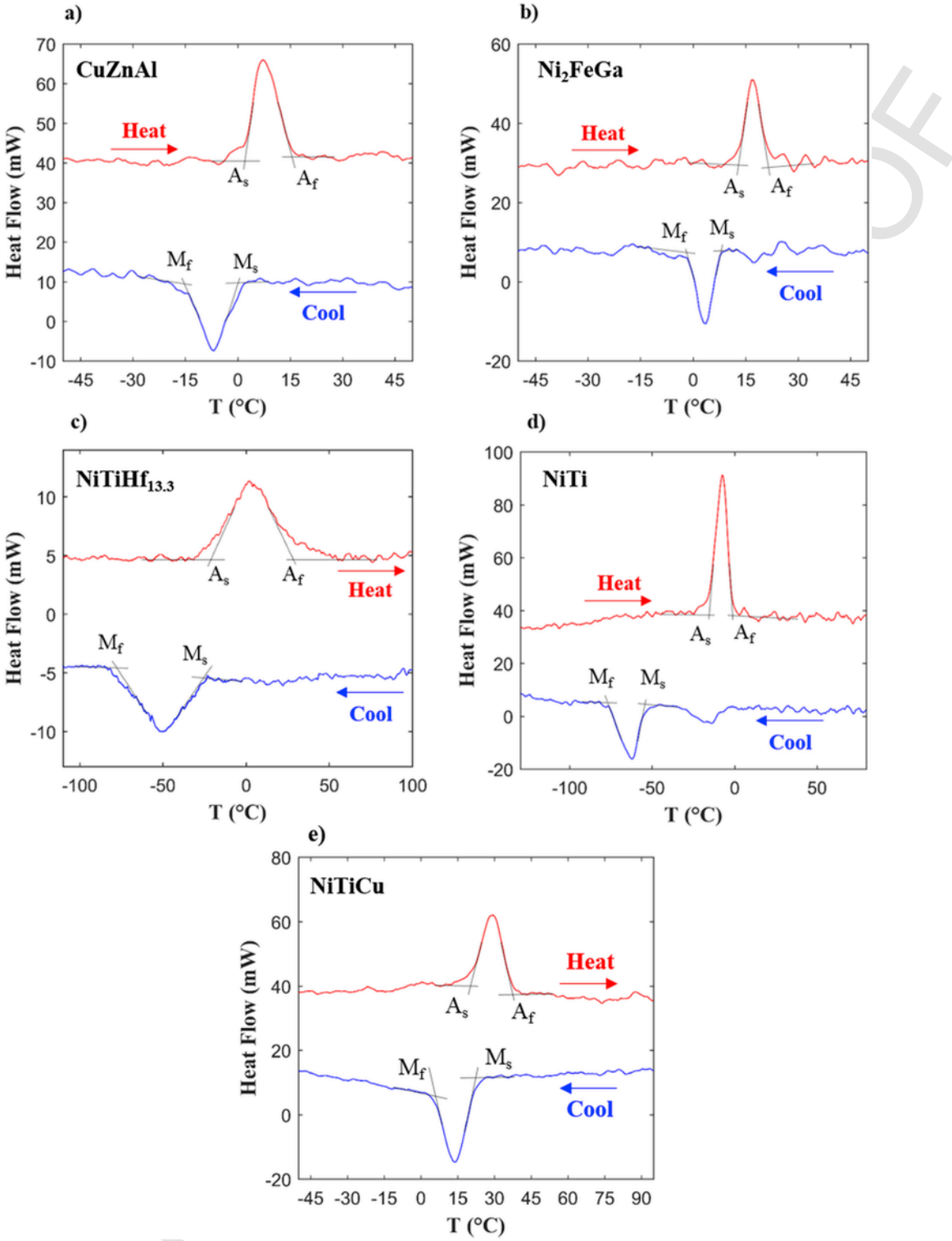

Fig. 15. a) DSC results of CuZnAl, b) Ni_2FeGa, c) $NiTiHf_{13.3}$, d) NiTi, and e) NiTiCu SMAs. The transformation temperatures, M_s, M_f, A_s, and A_f, are marked on the DSC curves for each material.

the Frederick Seitz Materials Research Laboratory Central Research Facilities, University of Illinois. The authors are grateful to Mr. Changgong Kim for his assistance with the EBSD analysis. The single crystals were grown by Prof. Yuriy Chumlyakov of Tomsk State University, Russia.

Table 2
The ΔS and ΔT_{th} calculated from Method I using the Clausius-Clapeyron slopes, $\frac{d\sigma_E}{dT}$, for CuZnAl, Ni_2FeGa, $NiTiHf_{13.3}$ and NiTi in tension, where σ_E is defined as the average of σ_F and σ_R.

Method I (Tension)	$d\sigma_F/dT$ MPa/°C	$d\sigma_E/dT$ MPa/°C	ε_T %	ΔS^{CC} J/kg K	T K	ΔT_{th} K	ΔT_{max} K
CuZnAl	2.01	2.05	10	−20.5	348	16.9	14.2
Ni_2FeGa	0.99	1.01	14.5	−14.6	403	12.8	10.1
$NiTiHf_{13.3}$	5.1	5.08	12.4	−63.0	318	35.1	6.95
NiTi	7.02	7.03	7.5	−52.7	338	30.2	18.2

Table 3
The ΔS and ΔT_{th} calculated from Method I using the Clausius-Clapeyron slopes, $\frac{d\sigma_E}{dT}$, for CuZnAl, Ni_2FeGa, NiTiCu and NiTi in compression.

Method I (Compression)	$d\sigma_F/dT$ MPa/°C	$d\sigma_E/dT$ MPa/°C	ε_T %	ΔS^{CC} J/kg K	T K	ΔT_{th} K	ΔT_{max} K
CuZnAl	2.87	2.94	8.1	−23.8	383	21.7	13.1
Ni_2FeGa	3.78	3.79	6.3	−23.9	403	20.9	13.5
NiTiCu	6.17	6.2	5.55	−34.4	323	19.8	15.2
NiTi	8.82	8.83	6.5	−57.4	338	32.9	18.2

Table 4
The ΔT_{th} calculated from Method II by using enthalpy changes, ΔH, from martensite to austenite phase transformation for CuZnAl, Ni_2FeGa, $NiTiHf_{13.3}$, NiTiCu, and NiTi. T_p is the peak temperature corresponding to the reverse martensitic transformation (M to A) shown in the DSC curve. ΔS_{th}^{Tp} is calculated using T_p and ΔT_{th}^{Tp} is evaluated from Ref. ΔS_{th}^{Tp}[44]. The ΔT_{th} is determined using the equilibrium temperature T_o.

Method II	ΔH J/g	T_o K	T_p K	T K	ΔS^{DSC} J/kg K	ΔS_{Tp}^{DSC} J/kg K	ΔT_{th} K	ΔT_{th}^{Tp} K	ΔT_{max} K
CuZnAl	6.69	284	280	348	−23.6	−23.9	19.5	19.8	14.2
Ni_2FeGa	5.67	287	290	403	−19.8	−19.5	17.3	17.1	13.5
$NiTiHf_{13.3}$	15.9	265	273	318	−60.0	−58.2	32.3	32.5	6.95
NiTi	12.7	245.5	268	338	−51.7	−47.4	29.6	27.1	18.2
NiTiCu	11.3	299	302	323	−37.8	−37.4	21.8	21.6	15.2

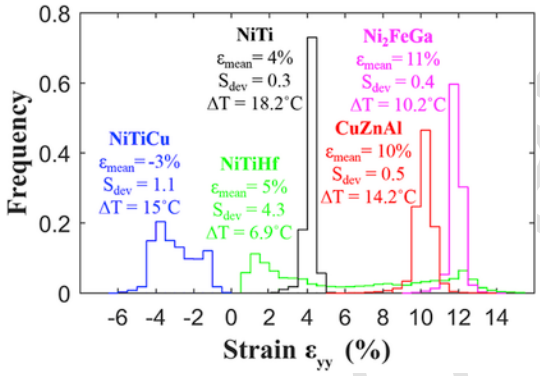

Fig. 16. The histogram indicates the distribution of local strains within each material. The frequency represents the fraction of a sample that exhibits a particular strain value. The increase in the width of the histograms indicates an increased level of transformation heterogeneity developing in the material. This is also recognized by noticing the increase in the standard deviation (Sdev) given in the figure for each histogram. The experimentally measured temperature changes for each material are listed as well.

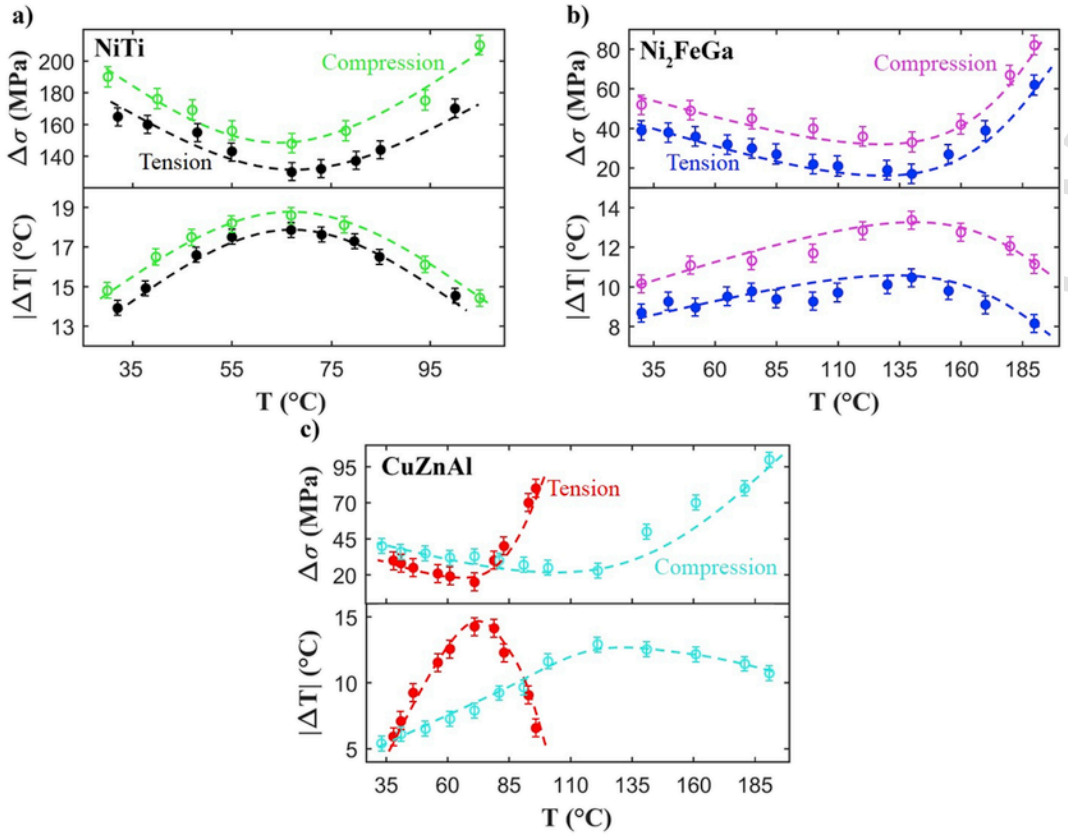

Fig. 17. The correlation between stress hysteresis and temperature change capability as a function of isothermal test temperatures for a) NiTi, b) Ni_2FeGa, and c) CuZnAl under both compressive and tensile loading state. The dashed line are added in order to aid the eyes.

References

[1] H. Ossmer, S. Miyazaki, M. Kohl, Elastocaloric heat pumping using a shape memory alloy foil device, In: 2015 Transducers-2015 18th International Conference on Solid-state Sensors, Actuators and Microsystems (TRANSDUCERS), IEEE, 2015, pp. 726–729.

[2] S. Qian, Y. Wu, J. Ling, J. Muehlbauer, Y. Hwang, I. Takeuchi, et al., Design, development and testing of a compressive thermoelastic cooling prototype, In: 24th International Congress of Refrigeration (ICR2015), Yokohama, Jp, 2015. submitted for publication.

[3] M. Schmidt, J. Ullrich, A. Wieczorek, J. Frenzel, A. Schütze, G. Eggeler, et al., Thermal stabilization of NiTiCuV shape memory alloys: observations during elastocaloric training, Shape Mem. Superelasticity 1 (2015) 132–141.

[4] J. Cui, Y. Wu, J. Muehlbauer, Y. Hwang, R. Radermacher, S. Fackler, et al., Demonstration of high efficiency elastocaloric cooling with large ΔT using NiTi wires, Appl. Phys. Lett. 101 (2012) 073904.

[5] J. Tušek, K. Engelbrecht, L.P. Mikkelsen, N. Pryds, Elastocaloric effect of Ni-Ti wire for application in a cooling device, J. Appl. Phys. 117 (2015) 124901.

[6] L. Mañosa, S. Jarque-Farnos, E. Vives, A. Planes, Large temperature span and giant refrigerant capacity in elastocaloric Cu-Zn-Al shape memory alloys, Appl. Phys. Lett. 103 (2013) 211904.

[7] H. Ossmer, C. Chluba, M. Gueltig, E. Quandt, M. Kohl, Local evolution of the elastocaloric effect in TiNi-based films, Shape Mem. Superelasticity 1 (2015) 142–152.

[8] C. Bechtold, C. Chluba, R.L. De Miranda, E. Quandt, High cyclic stability of the elastocaloric effect in sputtered TiNiCu shape memory films, Appl. Phys. Lett. 101 (2012) 091903.

[9] L. Mañosa, A. Planes, Materials with giant mechanocaloric effects: cooling by strength, Adv. Mater. (2016).

[10] L. Manosa, A. Planes, Mechanocaloric Effects in Shape Memory Alloys, 2016. arXiv preprint arXiv:160303658.

[11] G.J. Pataky, E. Ertekin, H. Sehitoglu, Elastocaloric cooling potential of NiTi, Ni 2 FeGa, and CoNiAl, Acta Mater. 96 (2015) 420–427.

[12] S. Miyazaki, T. Imai, Y. Igo, K. Otsuka, Effect of cyclic deformation on the pseudoelasticity characteristics of Ti-Ni alloys, Metall. Trans. A 17 (1986) 115–120.

[13] S. Miyszaki, K. Otsuka, Y. Suzuki, Tansformation pseudoelasticity and deformation behavior in a Ti-50.6 at%.Ni alloy, Scr. Metall. 15 (1981) 287–292.

[14] R. Hamilton, H. Sehitoglu, Y. Chumlyakov, H. Maier, Stress dependence of the hysteresis in single crystal NiTi alloys, Acta Mater. 52 (2004) 3383–3402.

[15] Y.I. Chumlyakov, I. Kireeva, I. Karaman, E.Y. Panchenko, E. Zakharova, A. Tverskov, et al., Orientational dependence of shape memory effects and superelasticity in CoNiGa, NiMnGa, CoNiAl, FeNiCoTi, and TiNi single crystals, Russ. Phys. J. 47 (2004) 893–911.

[16] D. Soto-Parra, E. Vives, L. Mañosa, J. Matutes-Aquino, H. Flores-Zúñiga, A. Planes, Elastocaloric effect in Ti-Ni shape-memory wires associated with the B2↔ B19'and B2↔ R structural transitions, Appl. Phys. Lett. 108 (2016) 071902.

[17] W. Abuzaid, H. Sehitoglu, J. Lambros, Plastic strain localization and fatigue micro-crack formation in Hastelloy X, Mater. Sci. Eng. A 561 (2013) 507–519.

[18] M. Kimiecik, J. Jones, S. Daly, Grain orientation dependence of martensitic phase transformation in polycrystalline shape memory alloys, Acta Mater 94 (2015) 214–223.

[19] Y. Wu, L. Patriarca, G. Li, H. Sehitoglu, Y. Soejima, T. Ito, et al., Shape memory response of polycrystalline NiTi12. 5Hf alloy: transformation at small scales, Shape Mem. Superelasticity 1 (2015) 387–397.

[20] L. Patriarca, H. Sehitoglu, E.Y. Panchenko, Y. Chumlyakov, High-temperature functional behavior of single crystal Ni 51.2 Ti 23.4 Hf 25.4 shape memory alloy, Acta Mater. 106 (2016) 333–343.

[21] Y. Wu, L. Patriarca, H. Sehitoglu, Y. Chumlyakov, Ultrahigh tensile transformation strains in new Ni 50.5 Ti 36.2 Hf 13.3 shape memory alloy, Scr. Mater. 118 (2016) 51–54.

[22] A. Ojha, H. Sehitoglu, Twinning stress prediction in bcc metals and alloys, Philos. Mag. Lett. 94 (2014) 647–657.

[23] A. Ojha, H. Sehitoglu, L. Patriarca, H. Maier, Twin migration in Fe-based bcc crystals: theory and experiments, Philos. Mag. 94 (2014) 1816–1840.

[24] E. Vives, S. Burrows, R.S. Edwards, S. Dixon, L. Mañosa, A. Planes, et al., Temperature contour maps at the strain-induced martensitic transition of a Cu–Zn–Al shape-memory single crystal, Appl. Phys. Lett. 98 (2011) 011902.
[25] H. Ossmer, F. Lambrecht, M. Gültig, C. Chluba, E. Quandt, M. Kohl, Evolution of temperature profiles in TiNi films for elastocaloric cooling, Acta Mater. 81 (2014) 9–20.
[26] K. Gall, N. Yang, H. Sehitoglu, Y.I. Chumlyakov, Fracture of precipitated NiTi shape memory alloys, Int. J. Fract. 109 (2001) 189–207.
[27] J. Pons, M. Sade, F. Lovey, E. Cesari, Pseudoelastic cycling and two-way shape memory effect in β Cu–Zn–Al alloys with γ-precipitates, Mater. Trans. JIM 34 (1993) 888–894.
[28] C. Efstathiou, H. Sehitoglu, P. Kurath, S. Foletti, P. Davoli, Fatigue response of NiFeGa single crystals, Scr. Mater. 57 (2007) 409–412.
[29] S. Nikitin, G. Myalikgulyev, M. Annaorazov, A. Tyurin, R. Myndyev, S. Akopyan, Giant elastocaloric effect in FeRh alloy, Phys. Lett. A 171 (1992) 234–236.
[30] F. Xiao, T. Fukuda, T. Kakeshita, Significant elastocaloric effect in a Fe-31.2Pd (at. %) single crystal, Appl. Phys. Lett. 102 (2013) 161914.
[31] F. Xiao, M. Jin, J. Liu, X. Jin, Elastocaloric effect in Ni 50 Fe 19 Ga 27 Co 4 single crystals, Acta Mater. 96 (2015) 292–300.
[32] B. Lu, F. Xiao, A. Yan, J. Liu, Elastocaloric effect in a textured polycrystalline Ni-Mn-In-Co metamagnetic shape memory alloy, Appl. Phys. Lett. 105 (2014) 161905.
[33] H. Sehitoglu, I. Karaman, R. Anderson, X. Zhang, K. Gall, H. Maier, et al., Compressive response of NiTi single crystals, Acta Mater. 48 (2000) 3311–3326.
[34] Y.I. Chumlyakov, I. Kireeva, E.Y. Panchenko, E. Timofeeva, Z. Pobedennaya, S. Chusov, et al., High-temperature superelasticity in CoNiGa, CoNiAl, NiFeGa, and TiNi monocrystals, Russ. Phys. J. 51 (2008) 1016–1036.
[35] K. Otsuka, C.M. Wayman, Shape Memory Materials, Cambridge University Press, 1999.
[36] M.A. Sutton, J.J. Orteu, H. Schreier, Image Correlation for Shape, Motion and Deformation Measurements: Basic Concepts, Theory and Applications, Springer Science & Business Media, 2009.
[37] T. Saburi, C. Wayman, K. Takata, S. Nenno, The shape memory mechanism in 18R martensitic alloys, Acta Metall. 28 (1980) 15–32.
[38] E. Bonnot, R. Romero, X. Illa, L. Mañosa, A. Planes, E. Vives, Hysteresis in a system driven by either generalized force or displacement variables: martensitic phase transition in single-crystalline Cu− Zn− Al, Phys. Rev. B 76 (2007) 064105.
[39] R. Hamilton, H. Sehitoglu, C. Efstathiou, H. Maier, Inter-martensitic transitions in Ni–Fe–Ga single crystals, Acta Mater. 55 (2007) 4867–4876.
[40] H. Sehitoglu, I. Karaman, X. Zhang, H. Kim, Y. Chumlyakov, I. Kireeva, et al., Deformation of NiTiCu shape memory single crystals in compression, Metal. Mater. Trans. A 32 (2001) 477–489.
[41] K. Otsuka, X. Ren, Physical metallurgy of Ti–Ni-based shape memory alloys, Prog. Mater. Sci. 50 (2005) 511–678.
[42] J. Wang, H. Sehitoglu, H. Maier, Dislocation slip stress prediction in shape memory alloys, Int. J. Plast. 54 (2014) 247–266.
[43] J. Wang, H. Sehitoglu, Modelling of martensite slip and twinning in NiTiHf shape memory alloys, Philos. Mag. 94 (2014) 2297–2317.
[44] K. Niitsu, Y. Kimura, X. Xu, R. Kainuma, Composition dependences of entropy change and transformation temperatures in Ni-rich Ti–Ni system, Shape Mem. Superelasticity 1 (2015) 124–131.
[45] T. Saburi, S. Nenno, The Shape Memory Effect and Related Phenomena. Solid to Solid Phase Transformations, 19811455–1479.
[46] H. Tong, C. Wayman, Characteristic temperatures and other properties of thermoelastic martensites, Acta Metall. 22 (1974) 887–896.
[47] Y. Sutou, N. Kamiya, T. Omori, R. Kainuma, K. Ishida, K. Oikawa, Stress-strain characteristics in Ni–Ga–Fe ferromagnetic shape memory alloys, Appl. Phys. Lett. 84 (2004) 1275–1277.
[48] C. Efstathiou, H. Sehitoglu, J. Carroll, J. Lambros, H.J. Maier, Full-field strain evolution during intermartensitic transformations in single-crystal NiFeGa, Acta Mater. 56 (2008) 3791–3799.
[49] P. Wollants, J. Roos, L. Delaey, Thermally-and stress-induced thermoelastic martensitic transformations in the reference frame of equilibrium thermodynamics, Prog. Mater. Sci. 37 (1993) 227–288.
[50] K. Gall, H. Sehitoglu, Y.I. Chumlyakov, I. Kireeva, Tension–compression asymmetry of the stress–strain response in aged single crystal and polycrystalline NiTi, Acta Mater. 47 (1999) 1203–1217.
[51] K. Gall, H. Sehitoglu, The role of texture in tension–compression asymmetry in polycrystalline NiTi, Int. J. Plast. 15 (1999) 69–92.
[52] G. Hahn, A. Rosenfield, Metallurgical factors affecting fracture toughness of aluminum alloys, Metall. Trans. A 6 (1975) 653–668.
[53] P. Chowdhury, H. Sehitoglu, A revisit to atomistic rationale for slip in shape memory alloys, Prog. Mater. Sci. 85 (2017) 1–42.
[54] P. Chowdhury, H. Sehitoglu, Deformation physics of shape memory alloys – fundamentals at atomistic frontier, Prog. Mater. Sci. 88 (2017) 49–88.
[55] H. Padilla, C. Smith, J. Lambros, A. Beaudoin, I. Robertson, Effects of deformation twinning on energy dissipation in high rate deformed zirconium, Metal. Mater. Trans. A 38 (2007) 2916–2927.
[56] M.S. Wechsler, D.S. Lieberman, T.A. Read, On theory of formation of martensite, J. Metals 5 (1953) 1503–1515.
[57] C. Efstathiou, H. Sehitoglu, Local transformation strain measurements in precipitated NiTi single crystals, Scr. Mater. 59 (2008) 1263–1266.